AD-A048 453 BALL BROS RESEARCH CORP BOULDER COLO AEROSPACE DIV F/G 9/5
MICROSTRIP ANTENNAS FOR MILLIMETER WAVES.(U)
OCT 77 M A WEISS DAAB07-76-C-0110
UNCLASSIFIED F77-07 ECOM-76-0110-F NL

1 OF 1
ADA048453

END
DATE FILMED
2-78
DDC

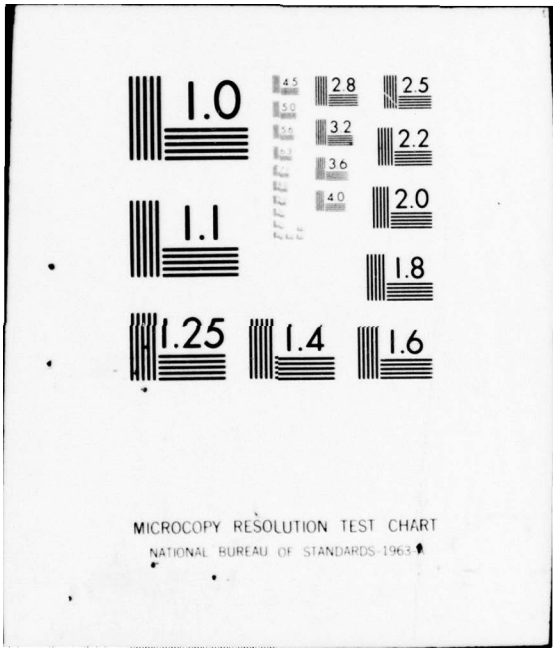
1.0
1.1
1.25
1.4
1.6
1.8
2.0
2.2
2.5
2.8
3.2
3.6
4.0
4.5
5.0
5.6
MICROCOPY RESOLUTION TEST CHART
NATIONAL BUREAU OF STANDARDS-1963-A

(12)
P.S.

Research and Development Technical Report

ECOM-76-0110-F

MICROSTRIP ANTENNAS FOR MILLIMETER WAVES

Michael A. Weiss
BALL BROTHERS RESEARCH CORP
Aerospace Division
Boulder, Colorado 80306

October 1977

Final Report for Period 1 Apr 1976 - 31 March 1977

Prepared for:

ECOM

ARMY ELECTRONICS COMMAND FORT MONMOUTH, NEW JERSEY 07703

HISA FM 2957-73

NOTICES

Disclaimers

The findings in this report are not to be construed as an official Department of the Army position, unless so designated by other authorized documents.

The citation of trade names and names of manufacturers in this report is not to be construed as official Government indorsement or approval of commercial products or services referenced herein.

Disposition

Destroy this report when it is no longer needed. Do not return it to the originator.

SECURITY CLASSIFICATION OF THIS PAGE (When Data Entered)

REPORT DOCUMENTATION PAGE

READ INSTRUCTIONS BEFORE COMPLETING FORM

1. REPORT NUMBER: ECOM-76-0110-F	2. GOVT ACCESSION NO.
3. RECIPIENT'S CATALOG NUMBER	
4. TITLE (and Subtitle): MICROSTRIP ANTENNAS FOR MILLIMETER WAVES,	5. TYPE OF REPORT & PERIOD COVERED: Final Report. 1 Apr 1976-31 Mar 1977,
	6. PERFORMING ORG. REPORT NUMBER: F77-07
7. AUTHOR(s): Michael A. Weiss	8. CONTRACT OR GRANT NUMBER(s): DAAB07-76-C-0110
9. PERFORMING ORGANIZATION NAME AND ADDRESS: Ball Brothers Research Corporation, Aerospace Division, Box 1062, Boulder, Colorado 80306	10. PROGRAM ELEMENT, PROJECT, TASK AREA & WORK UNIT NUMBERS: 611102 H48 21101
11. CONTROLLING OFFICE NAME AND ADDRESS: US Army Electronics Command, ATTN: DRSEL-NL-RH-1, Fort Monmouth, NJ 07703	12. REPORT DATE: Oct 1977
	13. NUMBER OF PAGES: 52 (12, 60 P.)
14. MONITORING AGENCY NAME & ADDRESS (if different from Controlling Office)	15. SECURITY CLASS. (of this report): Unclassified
	15a. DECLASSIFICATION/DOWNGRADING SCHEDULE

16. DISTRIBUTION STATEMENT (of this Report)

Approved for public release, distribution unlimited.

17. DISTRIBUTION STATEMENT (of the abstract entered in Block 20, if different from Report)

18. SUPPLEMENTARY NOTES

19. KEY WORDS (Continue on reverse side if necessary and identify by block number)

Microstrip Array, Millimeter Waves, Coax/Microstrip Transition, Waveguide/Microstrip Transition

20. ABSTRACT (Continue on reverse side if necessary and identify by block number)

This study was conducted to demonstrate the feasibility of low cost, conformal, printed circuit board arrays at millimeter frequencies. Development was concentrated in three basic areas: waveguide to microstrip transitions, a 4x4 element array at 35 GHz, and a 4x4 array at 60 GHz. The program was successful in each area of investigation.

DD FORM 1 JAN 73 1473 EDITION OF 1 NOV 65 IS OBSOLETE

Unclassified

SECURITY CLASSIFICATION OF THIS PAGE (When Data Entered)

409 767

SUMMARY

The study was conducted to demonstrate the feasibility of low-cost, conformal, printed circuit board arrays. Development was concentrated in three basic areas: waveguide to microstrip transitions, a 4x4 element array at 35 GHz, and a 4x4 array at 60 GHz. The program was successful in each area of investigation.

- Waveguide iris and probe-type transitions were investigated. The probe-type transition is presently being employed at 60 GHz while both coaxial and probe-type transitions are being used at 35 GHz.

- Two variations of a 35 GHz 4x4 element array were developed, fabricated and tested. Results demonstrate the feasibility of microstrip millimeter arrays at 35 GHz with efficiencies of approximately 77%.

- Two variations of a 60 GHz 4x4 element array were developed, fabricated and tested. Results demonstrate the feasibility of microstrip millimeter arrays at 60 GHz with efficiencies of approximately 78%.

BBRC has significantly advanced the microstrip millimeter array technology in all areas of design, including simplicity in design, monolithic in construction, conformal in mounting, and at relatively low cost.

TABLE OF CONTENTS

CONTENTS (Continued)

ILLUSTRATIONS

CONTENTS (Continued)

ILLUSTRATIONS

TABLES

Section 1
THEORY OF MICROSTRIP

1.1 BASIC MICROSTRIP ANTENNA CONFIGURATION

The linearly polarized microstrip element is basically a two-slot radiator[1] as shown in Figure 1-1. The two slots are separated

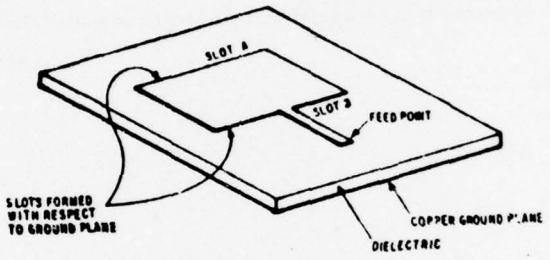

Figure 1-1 Linearly Polarized Microstrip Element

by a length of very low impedance transmission line. The length of this line can be made just short of a half wavelength so that the complex admittance G_s of Slot A is transformed to G_s at Slot B where it is added in parallel with the admittance G_s of Slot B. The result is a real admittance corresponding to the radiation admittance of the antenna plus a small loss component.

Losses depend mostly on the loss tangent of the dielectric material and to a lesser degree on thickness of the dielectric material and the conductivity of the conducting surfaces. The dimensions of the cavity may be expressed analytically as:

$$L_{slot} \approx \frac{\lambda}{2} \left(\frac{1}{\sqrt{\varepsilon}_r}\right) \qquad (1\text{-}1)$$

$$L_{cavity} \approx \frac{\lambda}{2} \left(\frac{K}{\sqrt{\varepsilon}_r}\right), \text{ for } K<1 \qquad (1\text{-}2)$$

[1] R.E. Munson, "Conformal Microstrip Antennas and Microstrip Phased Arrays," IEEE Transactions on Antennas and Propagation, Vol. AP-22, No. 1, January 1974, pp. 74-78.

where λ is the free space wavelength, K accounts for radiator edge capacitance, and ε_r is the real part of the dielectric constant.

Figure 1-2 is a sectional representation of the electric field

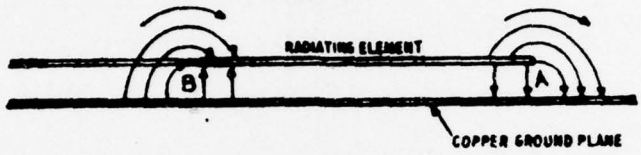

Figure 1-2 Electric Field in Vicinity of Microstrip Element

in the vicinity of a microstrip radiator. Since the element is about a half wavelength long in the dielectric, the field at one end of the microstrip cavity is reversed from that at the other end of the cavity. However, the radiated fields are in phase and tend to add in the broadside direction. Figure 1-3 shows a typical E-plane pattern attributable to these fields.

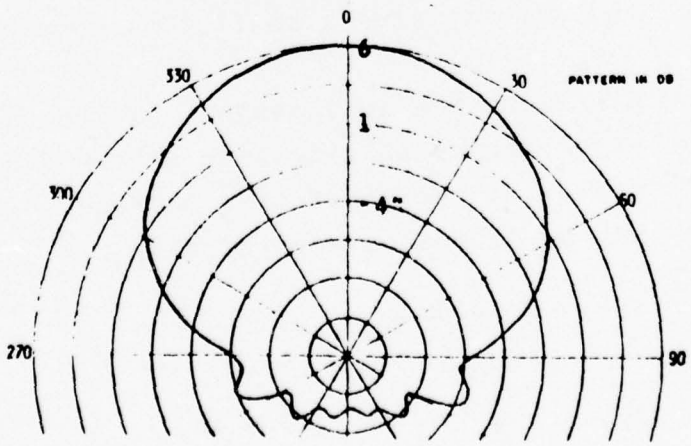

Figure 1-3 E-Plane Radiation Pattern of Linearly Polarized Microstrip Element

1.2 INPUT IMPEDANCE AND FEED NETWORKS

Microstrip antenna elements may be fed by a feed line etched on the same surface as the radiating element or by a feedthrough connection from the rear side of the circuit board.

For etched feed lines the line width required for a given characteristic impedance can be calculated using the well-known formulas for a narrow strip conductor above a conducting ground plane or by reference to an empirically-derived design curve.

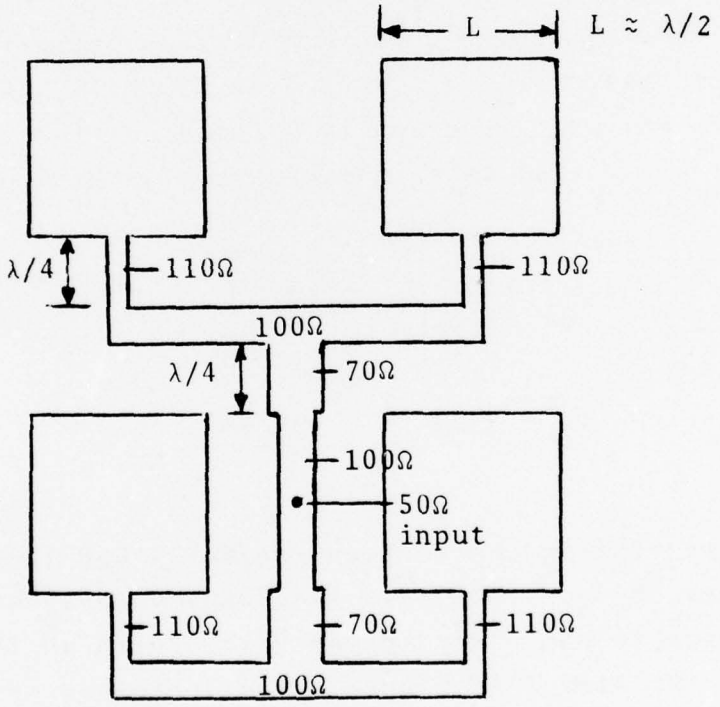

Figure 1-4 Typical Microstrip Feed Network

Figure 1-4 shows a typical feed network using quarterwave transformers to transform the driving impedance of the radiating element to that of the input port.

The microstrip radiator shown in Figure 1-4 is shown in cross-

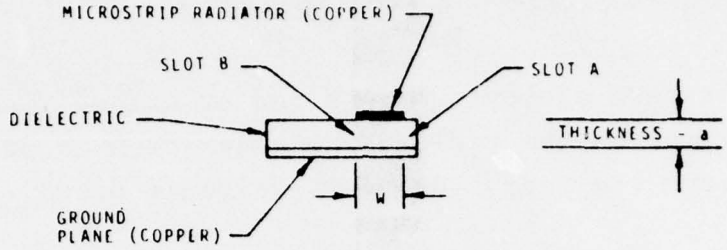

Figure 1-5 Microstrip Radiator - Cross Section View in E-Plane

section view in Figure 1-5. Gap A is an infinitesimal slot (in 0.010" microstrip $a/\lambda \approx 0.03$ at 35 GHz). The admittance of a slot radiator is given in Harrington[3] for small $ka(a/\lambda<0.1)$ which is always the case in microstrip antenna practice.

$$G_a \approx \frac{\pi}{\lambda\eta}\left[1 - \frac{(ka)^2}{24}\right] \tag{1-3}$$

$$B_a \approx \frac{3.135 - 2 \log ka}{\lambda\eta} \tag{1-4}$$

In most microstrip applications $ka/24<<1$ and the conductance simplifies to $G_a = \pi/\lambda\eta = 1/(\lambda \cdot 120\Omega m)$ or $R'_a = 120\lambda\ \Omega\cdot m$. The conductance is expressed in per unit length so that the resistance of the Slot A in Figure 1-5 is obtained by dividing R'_a by the length

$$R_a = \frac{R'a}{L} = \frac{120\lambda}{\lambda/2} = 240\Omega \tag{1-5}$$

[3] R.F. Harrington, Time Harmonic Electromagnetic Fields, New York, McGraw Hill, p. 276.

In the case of the microstrip radiator, the conductance and susceptance of Slots A and B are equal ($G_a = G_B$, $B_a = B_B$). However, when the admittance of slot B is transformed across the radiator to the feedpoint of slot A, it becomes conjugate complex provided the radiator width is chosen appropriately. Since the characteristic impedance of the transmission line formed by radiating element and ground plane is very low, the appropriate width deviates only slightly from $\frac{\lambda}{2}$. The admittance at the feedpoint then becomes:

$$Y_F = (G_a + iB_a) + (G_B - iB_B) \tag{1-6}$$

and since $B_a = B_b$ and $G_a = G_B$

$$Y_F = 2\ G_a \tag{1-7}$$

or $$R_F = \frac{1}{2G_a} = \frac{R_a}{2} = \frac{240}{2} = 120\Omega \tag{1-8}$$

In practice, this is the measured impedance. This theory is accurate in predicting the input impedances for many designs each with different frequencies, thicknesses, and radiator widths.

1.3 BANDWIDTH

The bandwidth of a microstrip antenna system is principally determined by the resonant radiating element. In terms of the dielectric thickness, t (inches) and the operating frequency, f_o (GHz) the bandwidth Δf (MHz) to the points at which the VSWR = 2.0:1 is given by the following empirically-derived equation

$$\Delta f = \frac{4f_o^2 t}{1/32} \quad (\text{MHz}) = 128 f_o^2 t \tag{1-9}$$

For antenna systems consisting of more than one resonant element, the bandwidth is also affected by the degree of coupling between the elements and their individual resonant frequencies. These effects are most conveniently handled by analysis of experimental results obtained during the development of specific antenna configurations.

Section 2
COAX AND WAVEGUIDE TO MICROSTRIP TRANSITIONS

2.1 COAX/MICROSTRIP TRANSITION

The coax/microstrip transition (Figure 2-1) was employed on the

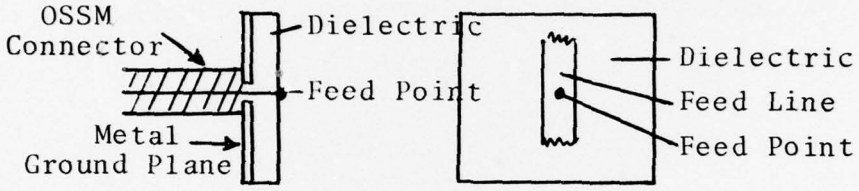

Figure 2-1 Coax/Microstrip Transition

35 GHz arrays because of its simplicity, ease in fabrication, and repeatability. This technique is identical to the typical approach used in microstrip antennas at lower frequencies. In this application an OSSM* coaxial connector is soldered to the ground plane, or backplate of the array. The inner conductor is extended through a hole in the dielectric substrate and soldered to the array feed network.

Omni Spectra, Incorporated data indicates an upper frequency limit of 38 GHz for OSSM* connectors due to higher order moding problems; therefore, operating problems in using OSSM* connectors would appear to be limited to insertion loss. Using Omni Spectra, Incorporated figures, maximum insertion loss is defined by

$$\text{Insertion Loss} = 0.03 \sqrt{\text{frequency (GHz)}} \text{ dBmax} \qquad (2\text{-}1)$$

This represents an insertion loss of approximately 0.18 dB maximum at 35 GHz.

* Subminiature connector similar in design and construction to the SMA series connectors.

2.2 WAVEGUIDE (IRIS)/MICROSTRIP TRANSITION

Due to the higher order moding problems in coaxial components above 38 GHz, and the common use of waveguide in millimeter applications, a program was undertaken to develop a practical waveguide-to-microstrip transition.

The waveguide iris approach shown in Figure 2-2 is a modification

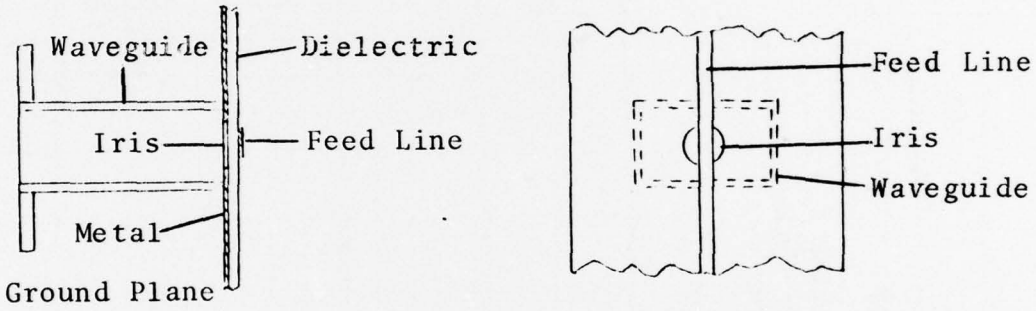

Figure 2-2 Waveguide (Iris)/Microstrip Transition

of a coaxial/waveguide transition scheme described in the "Waveguide Handbook"[4] authored by Dr. Marcuvitz. The thin aperture at the end of the waveguide (microstrip ground plane) excites the microstrip transmission line with an odd mode field pattern and provides a two-way power division with a 180° phase relation. The advantage in this design lies in the direct transition approach.

To facilitate fabrication, testing, and analysis, the iris waveguide/microstrip transition was first examined at 13 GHz. Figure 2-3 shows the waveguide return loss as a function of frequency. This return loss translates into a 2.0:1 VSWR bandwidth of approximately 65 MHz, compared to a 2.0:1 VSWR bandwidth of approximately 338 MHz for a microstrip radiator.

[4] N. Marcuvitz, Waveguide Handbook, Lexington, Massachusetts, Boston Technical Publishers, Inc., p. 174.

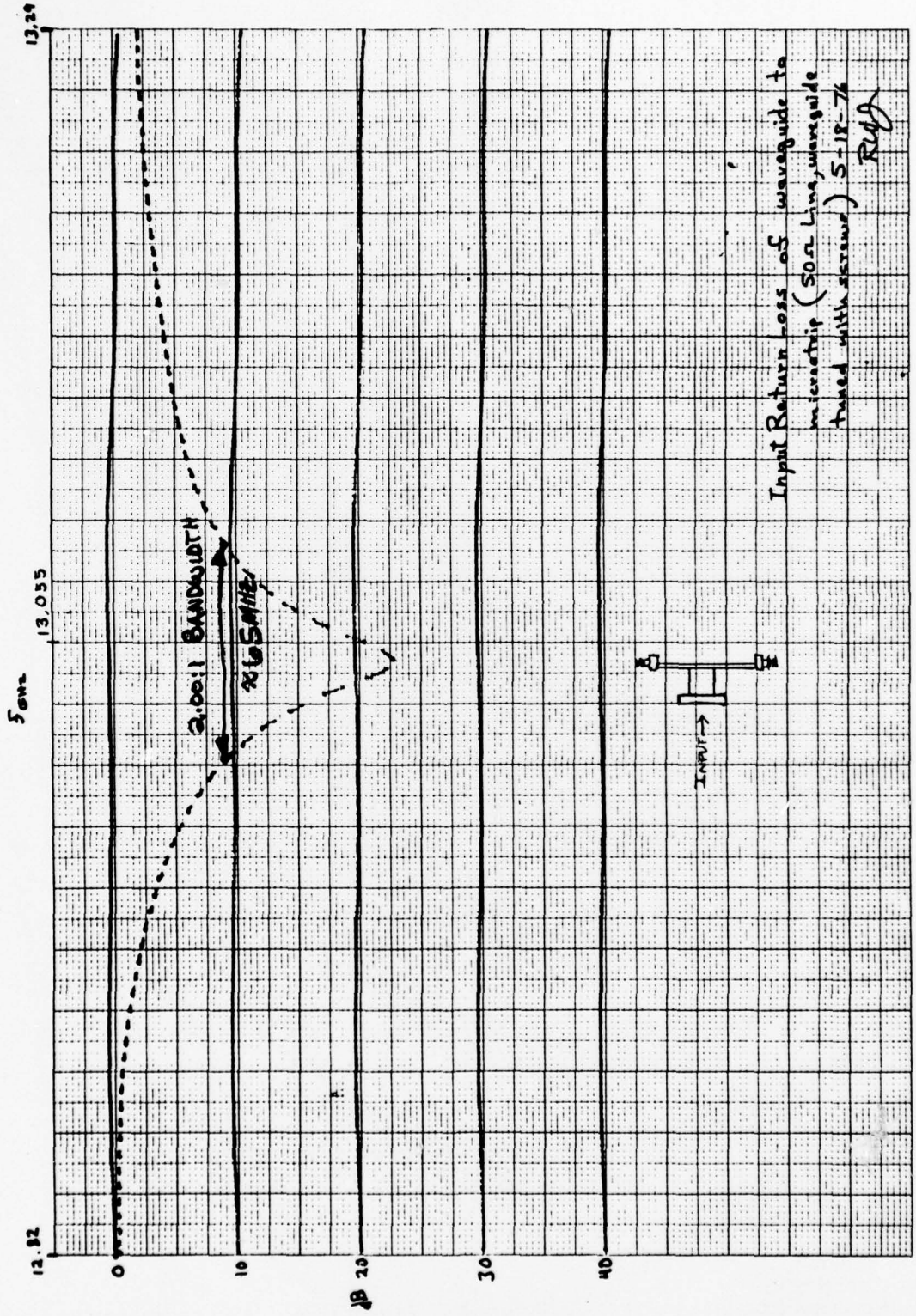

Figure 2-3 Return Loss of Iris Waveguide/Microstrip Transition

Insertion loss is shown in Figure 2-4 and is split 3.6 dB and 4.15 dB due to imbalance. These values convert to a total insertion loss of 0.85 dB at the optimum frequency for the iris transition. Another result predicted by theory is the 180^{o} phase difference caused by the odd mode excitation of the microstrip line. In actual use the feed point of the array must be located 180^{o} from the geometric center of the antenna array.

An attempt to increase bandwidth obtained with the circular iris transition was attempted at 13 GHz using a dumbell shaped window. The return loss data shown in Figure 2-5 indicates a good impedance match at a single frequency; however, bandwidth is still limited. 2.0:1 VSWR bandwidth is approximately 26 MHz, less than half that of the circular iris. Figure 2-6 shows insertion loss for the tuning of Figure 2-5, and also insertion loss for tuning to minimize insertion loss. Total insertion loss for these two cases are 1.9dB and 0.8dB, respectively.

2.3 WAVEGUIDE (PROBE)/MICROSTRIP TRANSITION

Investigation of the probe-type waveguide/microstrip transition shown in Figure 2-7 was undertaken when the narrow bandwidth characteristic of the iris-type transition became apparent. This design incorporates a probe located $\lambda/4$ from a short in the waveguide and the design is quite straightforward. Two tuning screws were used to tune out standing waves in the waveguide. Gold plated screws were used at 35 GHz and dielectric tuning screws were used at 60 GHz. Figure 2-8 shows return loss as a function of frequency for a waveguide probe type transition at 13.0 GHz. 2.0:1 VSWR bandwidth is greater than 400 MHz, which exceeds the expected 2.0:1 bandwidth of a microstrip radiator ($\approx$338 MHz). Insertion loss is shown in Figure 2-9 for two back-to-back transitions, indicating an approximate loss of less than 0.2 dB per transition over the 400 MHz frequency range.

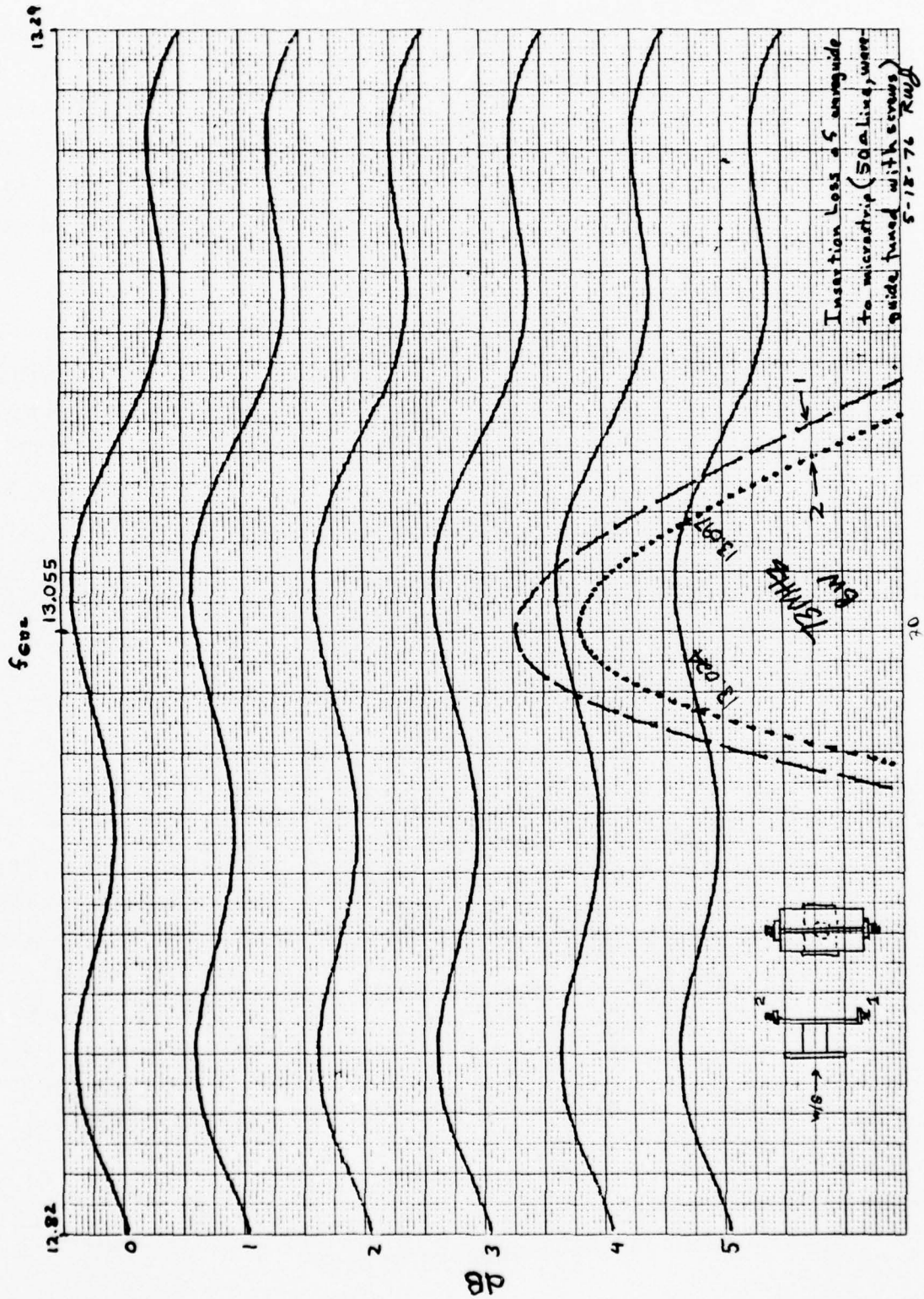

Figure 2-4 Insertion Loss of Iris Waveguide/Microstrip Transition

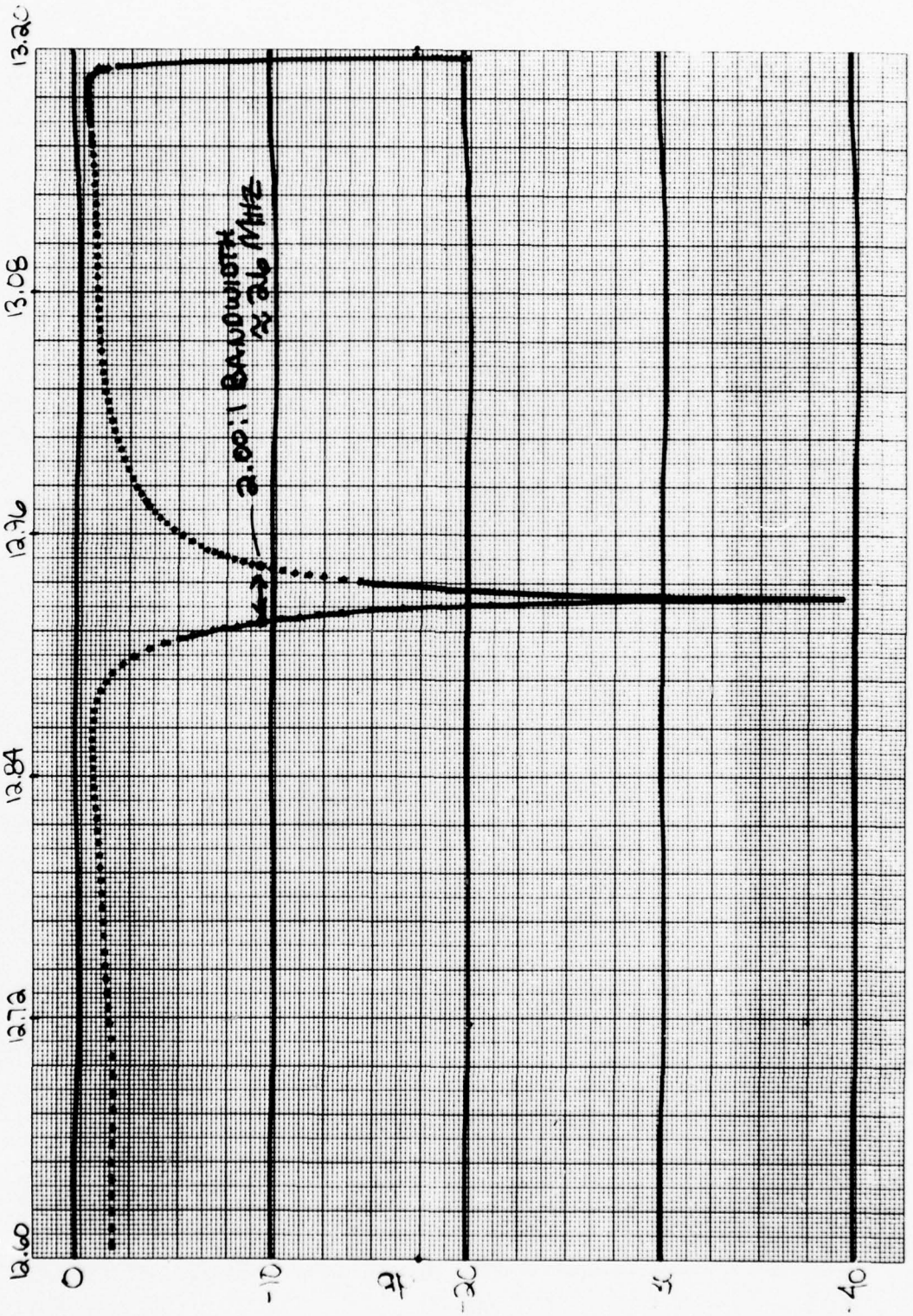

Figure 2-5 Return Loss of Dumbell Waveguide/Microstrip Transition

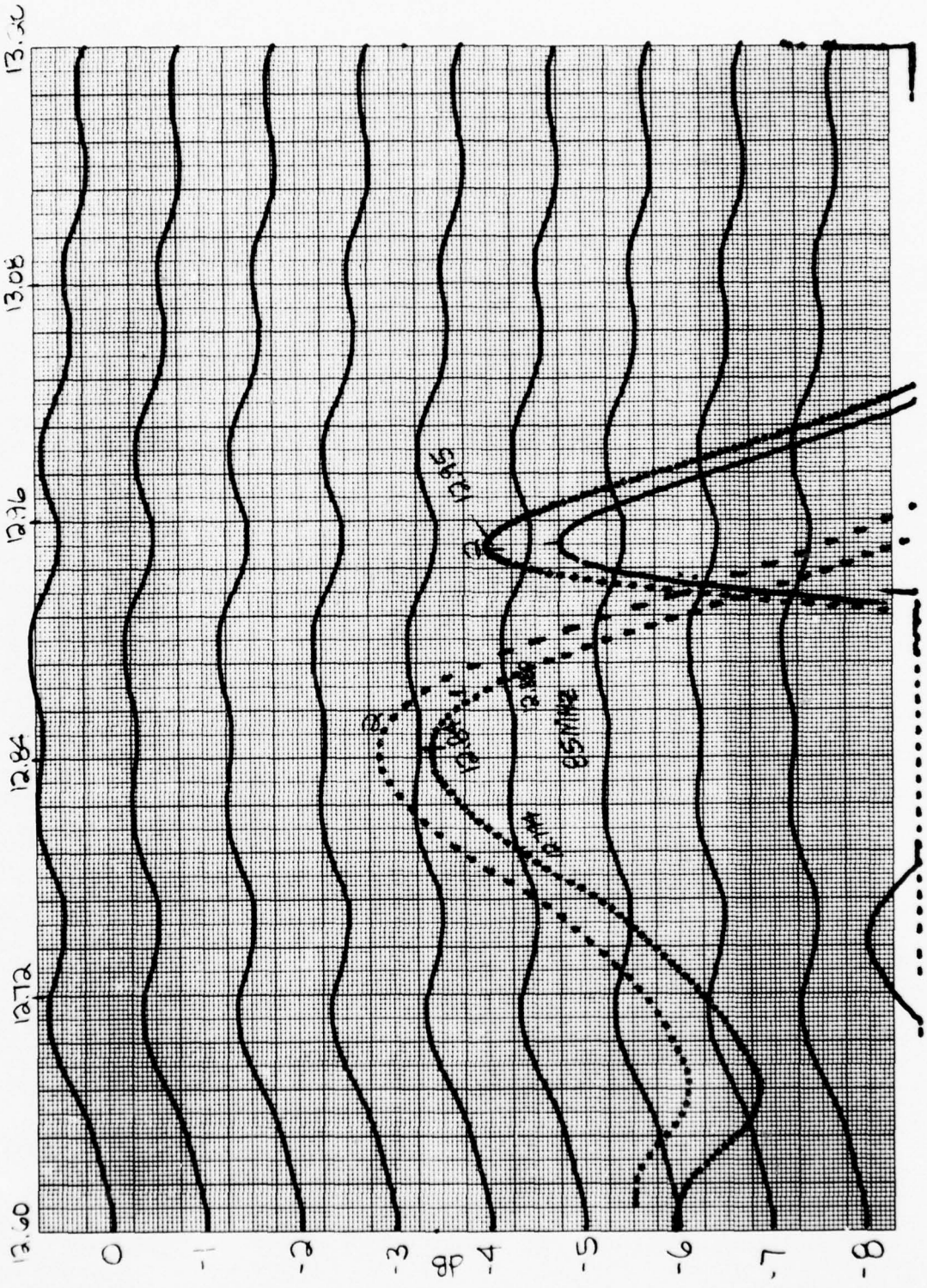

Figure 2-6 Insertion Loss of Dumbell Waveguide/Microstrip Transition

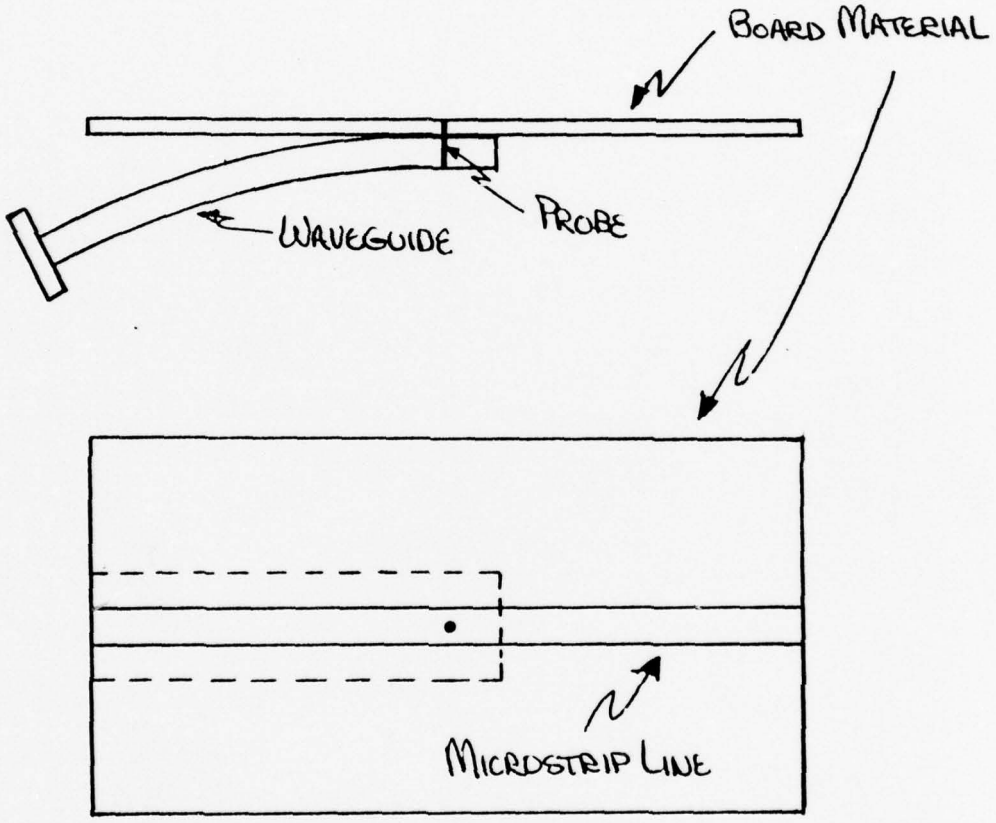

Figure 2-7 Waveguide (Probe)/Microstrip Transition

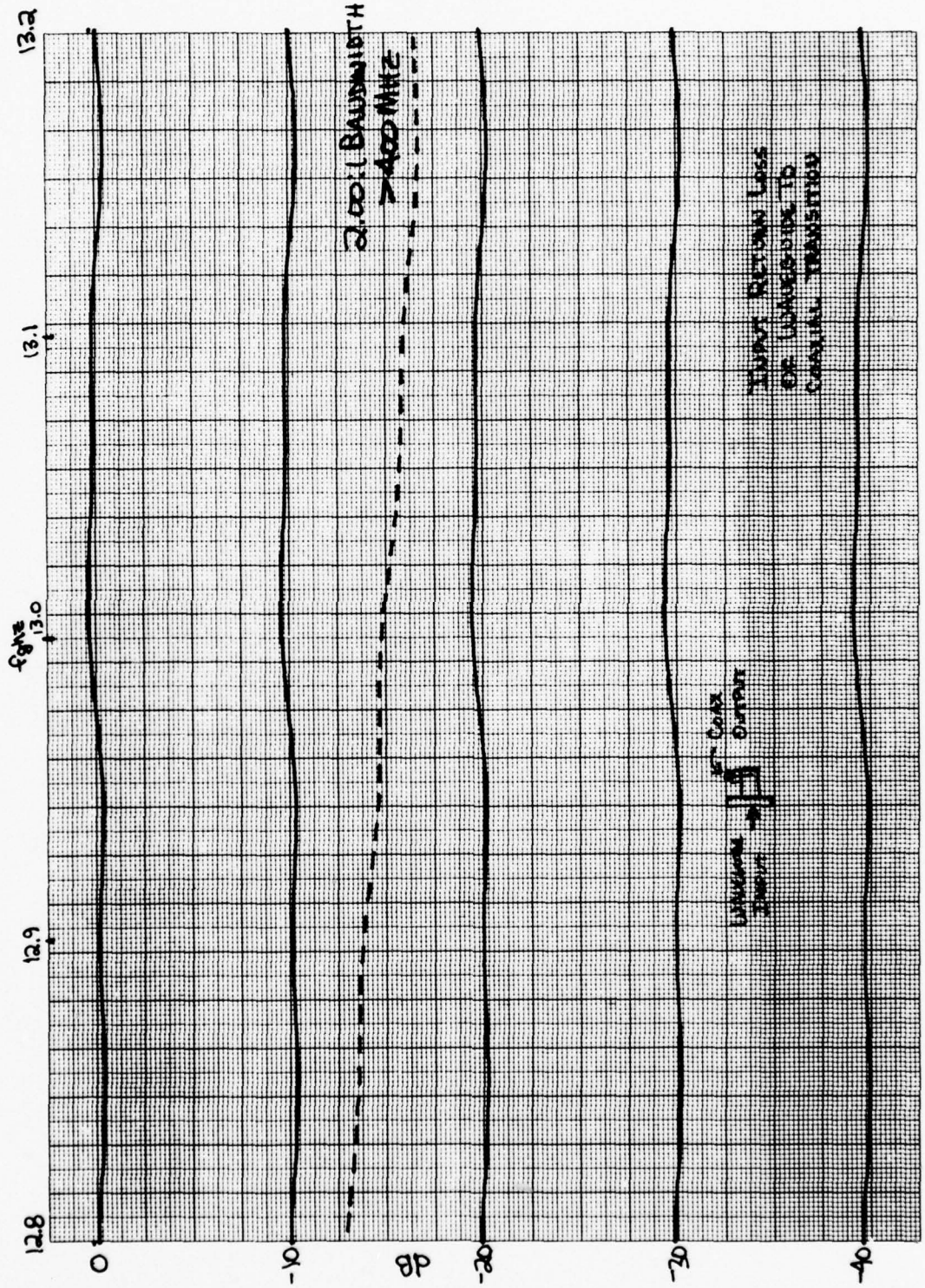

Figure 2-8 Return Loss of Waveguide/Coax Transition

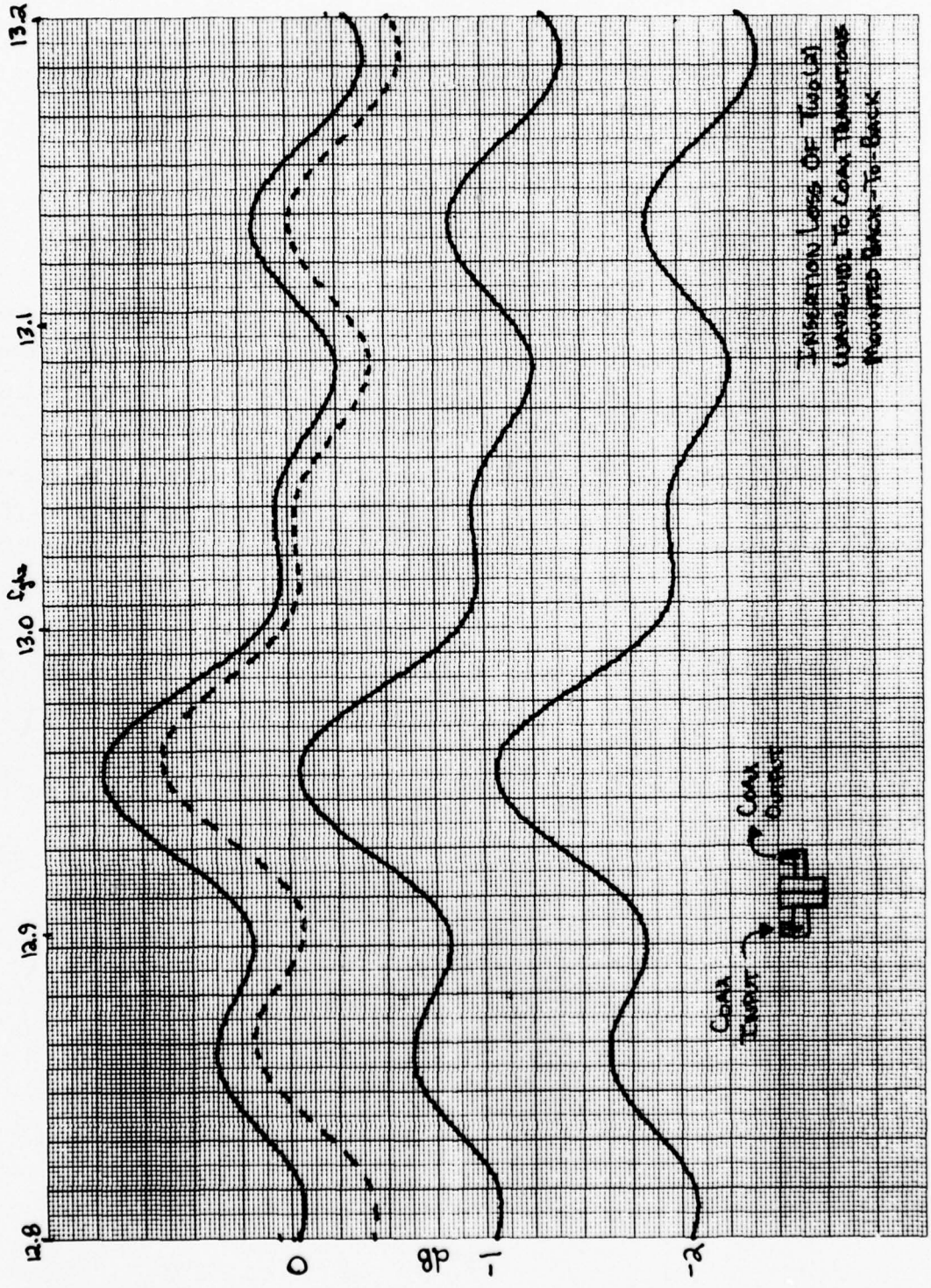

Figure 2-9 Insertion Loss of Waveguide/Coax Transition

2.4 TRANSITIONS - SUMMARY

Table 2-1 is a summary of bandwidth and insertion loss values at 13.0 GHz for the various transitions investigated.

Table 2-1

Transition Bandwidth and Insertion Loss
(13.0 GHz)

Transition Type	2.0:1 VSWR Bandwidth	Insertion Loss	Insertion Loss Bandwidth
Coaxial	>400 MHz	0.11 dB	Large
Waveguide Iris (Circular)	65 MHz	0.85 dB	Narrow
Waveguide Iris (Dumbell)	26 MHz	0.80 dB	Narrow
Waveguide Probe	>400 MHz	<0.20 dB	Large

Because the circular iris approach is more straightforward from a fabrication standpoint, both the waveguide iris and probe configurations were investigated at 35 GHz. Since equipment limitations prevented thorough measurements of transition performance at 35 GHz, a discussion of the array/transition combinations is included in Section 4 of this report.

Section 3
ETCHING

3.1 GLASS PLATE NEGATIVES

Repeatability problems with etching early in the study indicated a need to develop a highly refined etching technique for millimeter wave antennas. This problem was approached in two ways; first through the use of glass plate negatives, and secondly through a thinner copper cladding on the antenna substrates.

Since the 5 mil feed lines required in the 60 GHz arrays approach microcircuit dimensions, the microcircuit etching technique of using glass plate negatives was employed. These glass plates provide greater stability as well as higher resolution than the typically used film negatives.

3.2 COPPER THINNING

Another factor affecting tolerance during the etching procedure is "undercutting." Typically, it can be expected that undercutting at any etched edge will occur on a one-to-one proportion with the thickness of the copper cladding. With the standard 1 oz. (1.4 mil) copper cladding, this becomes a significant problem when considering the 5 to 10 mil feedlines employed in the 35 and 60 GHz arrays.

This situation was initially approached by developing a copper thinning technique which reduced the original 1 oz. (1.4 mil) copper cladding to approximately 1/2 oz. (0.7 mil).

Later in the study, BBRC obtained from the manufacturer a quantity of substrate material with 1/4 oz. (0.4 mil) copper cladding. Photographs of two 60 GHz arrays observed under identical magnification are shown in Figure 3-1. One array was etched on a 1 oz.

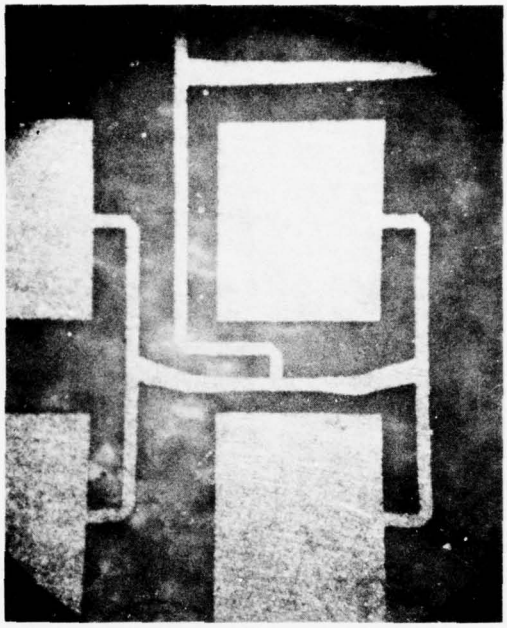

1/4 oz. Copper Cladding

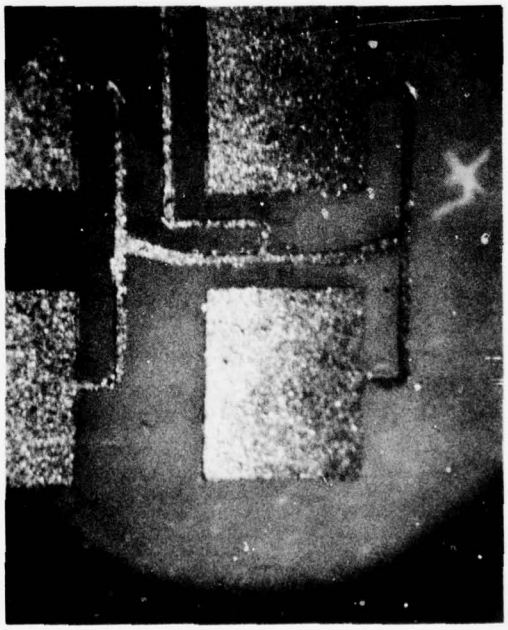

1 oz. Copper Cladding

Figure 3-1 Photographs of Etched Circuits

(1.4 mil) copper cladding while the other was etched on a 1/4 oz. (0.4 mil) copper cladding. The effects of undercutting are very obvious in these photographs. The 1/4 oz. (0.4 mil) copper cladding is essential in maintaining the high etching tolerances required for work in the millimeter wavelength region.

Section 4
35 GHz 4x4 ELEMENT ARRAYS

4.1 COAX FED SCALED ARRAY

The first 35 GHz 4x4 element array to be fabricated and tested was a scaled version of a 4x4 element array developed at 2.7 GHz. The array was originally developed at 2.7 GHz due to the difficulties involved in measuring performance parameters of individual array elements at 35 GHz. Figure 4-1 shows the measured H-plane radiation pattern of the 4x4 element array at 2.7 GHz.

The negative of this array was then reduced to the size required for operation at 35 GHz. The first 35 GHz 4x4 element array was etched on a 10 mil Duroid 5880 substrate having 1 oz. (1.4 mil) copper cladding. A photograph of this array is shown in Figure 4-2. Measured E and H plane radiation patterns are shown in Figures 4-3 and 4-4. These patterns compare very well with theoretical computer generated patterns which are shown in Figures 4-5 and 4-6. The array had an actual operating frequency of 36.6 GHz and was fed with a short section of 0.085" semirigid coaxial cable.

The following is an analysis of the array performance:

Theoretical Gain ($G = \frac{4\pi \text{ Area}}{\lambda^2}$)		17.84 dB
Measured Gain		16.00 dB
Loss in feed cable and connectors	$\approx$	0.40 dB
Mismatch loss (VSWR = 1.7:1)	$\approx$	0.30 dB
	Actual Gain	16.70 dB

Efficiency $\approx$ 17.84 dB - 16.70 dB $\approx$ 1.14 dB $\approx$ 77%

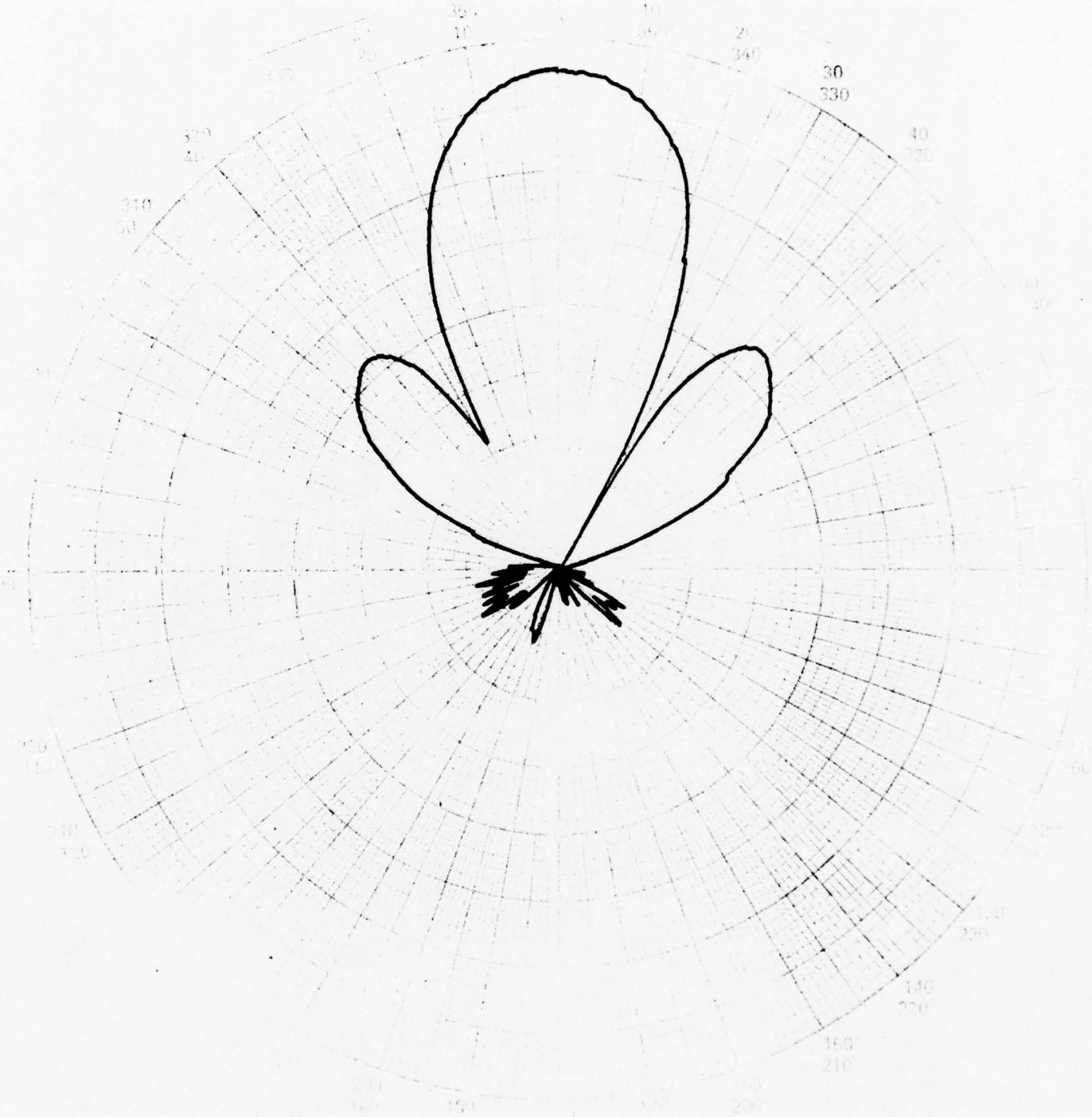

Figure 4-1 H-Plane Pattern of 4x4 Element Array (2.7 GHz)

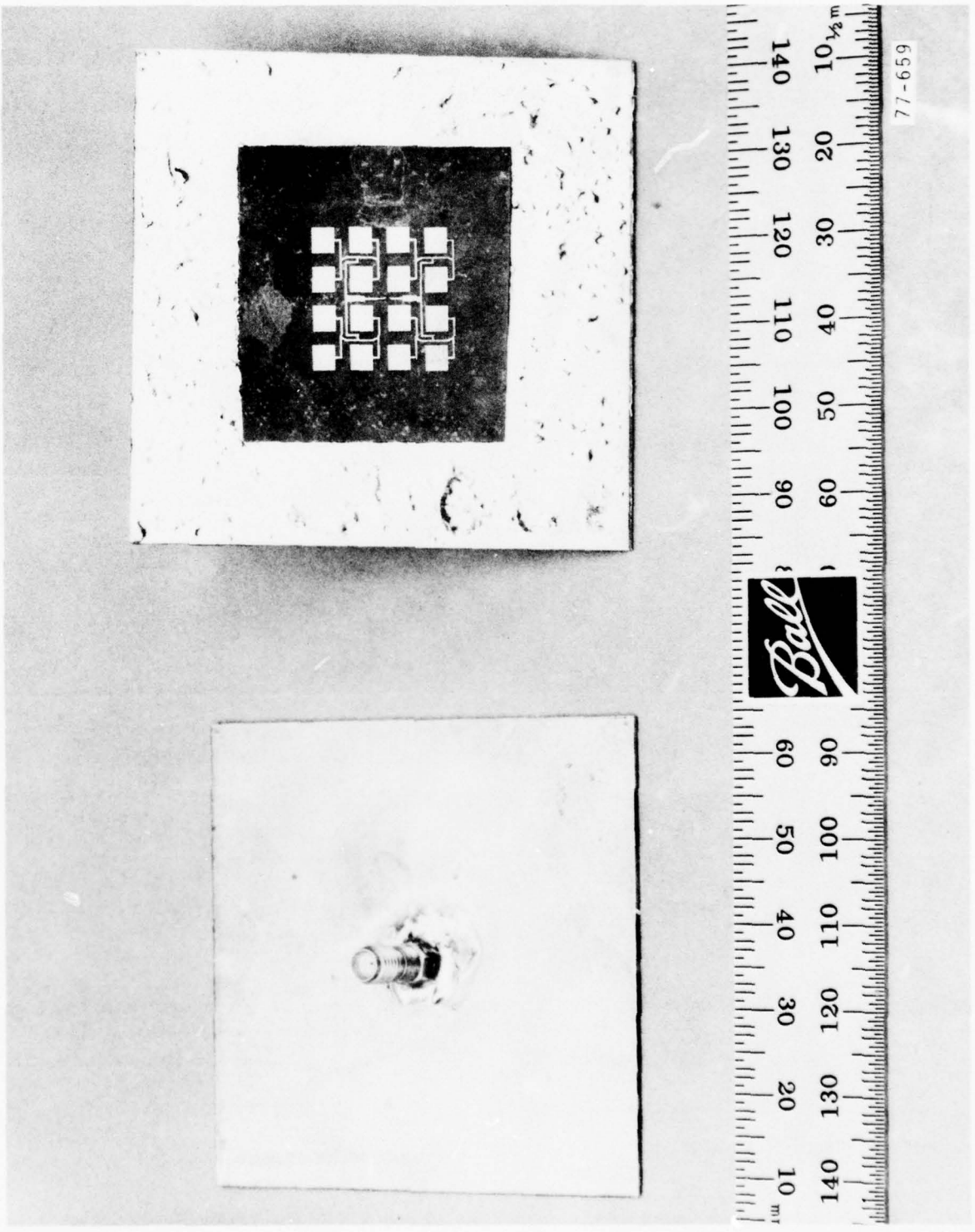

Figure 4-2 35 GHz Array

Figure 4-3 E-Plane Radiation Pattern (36.6 GHz) Coax Fed

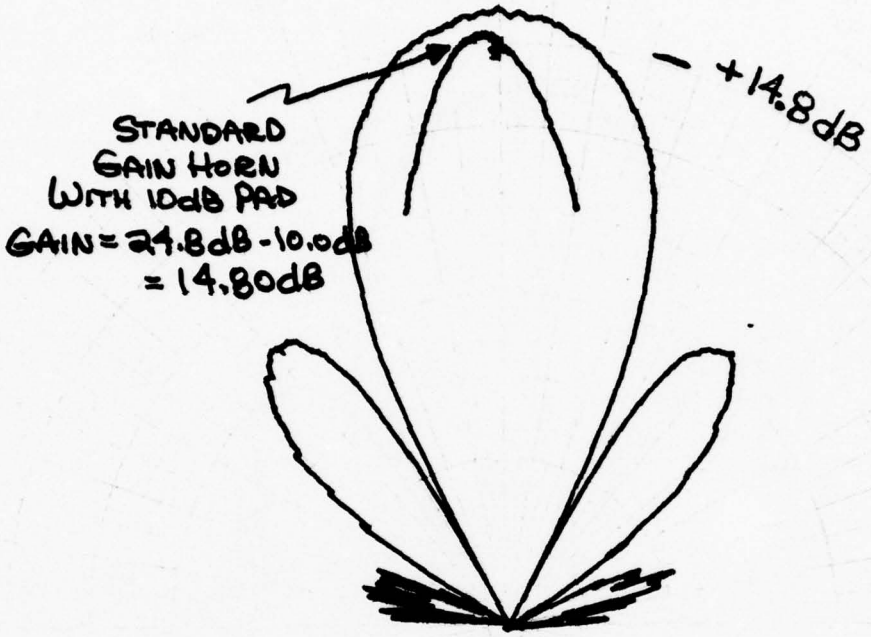

Figure 4-4 H-Plane Radiation Pattern (36.6 GHz) Coax Fed

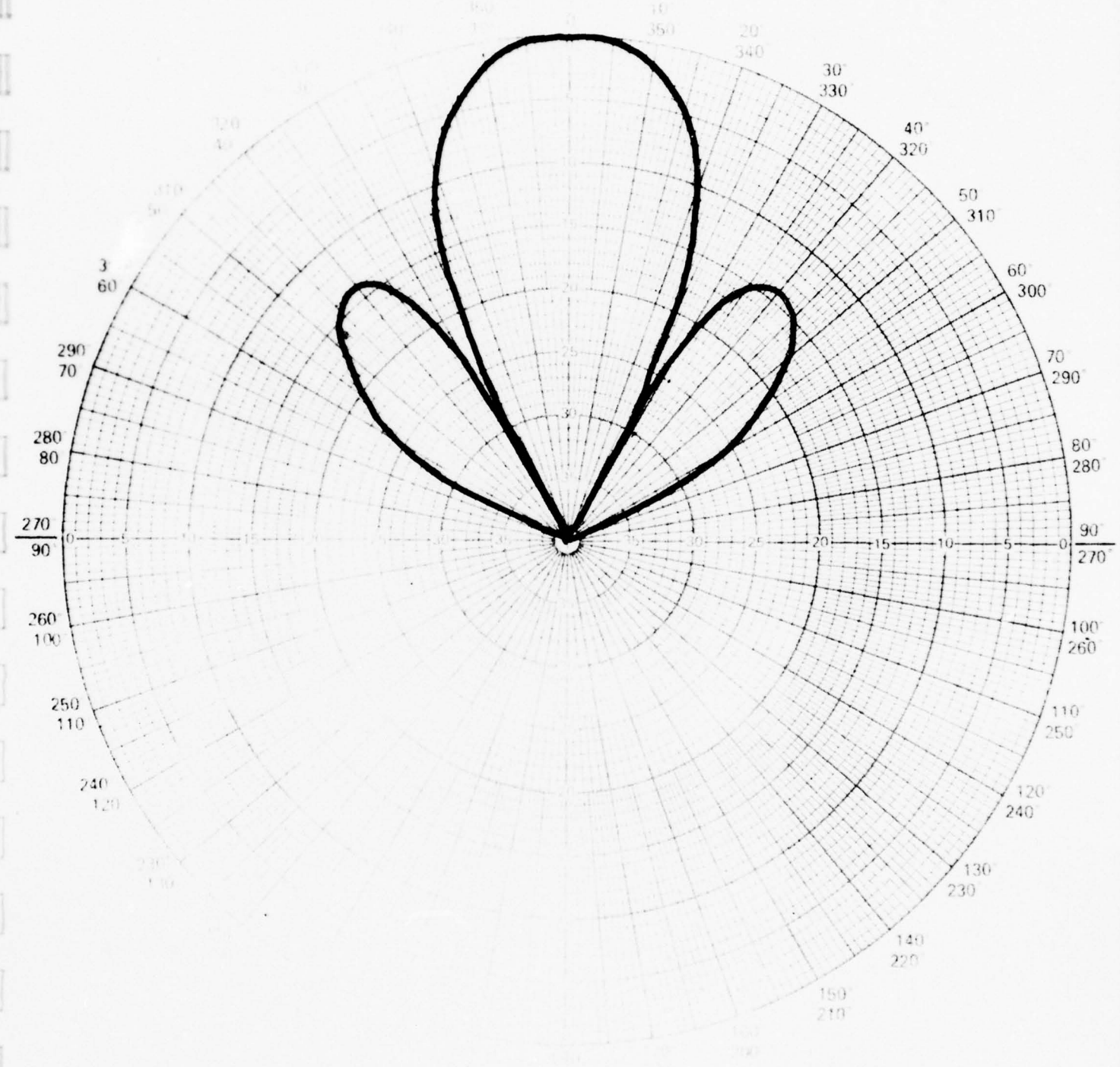

Figure 4-5 Computed E-Plane Radiation Pattern (36.6 GHz)

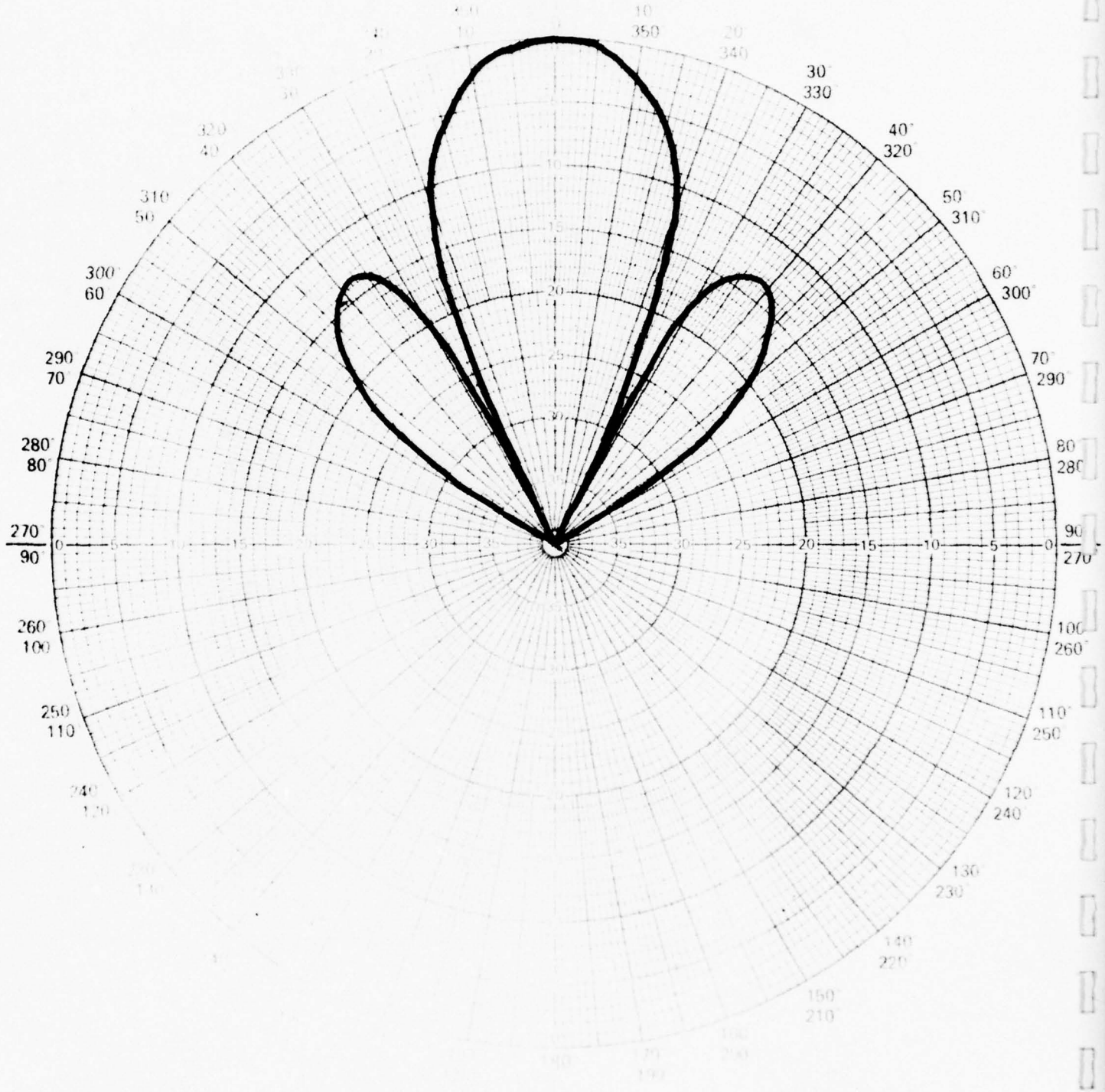

Figure 4-6 Computed H-Plane Radiation Pattern (36.6 GHz)

Losses resulting in the 77% efficiency can be attributed to dielectric loss and feedline radiation.

4.2 WAVEGUIDE PROBE FED SCALED ARRAY

Another test antenna was fabricated using the 4x4 element scaled array and the waveguide probe-type feed. The appearance of this antenna is similar to that shown in Figures 4-7 and 4-8. Measured E and H plane radiation patterns of this configuration are shown in Figures 4-9 and 4-10.

Following is an analysis of the array performance:

Theoretical Gain		17.84 dB
Measured Gain		13.30 dB
Loss in WG/microstrip transition	$\approx$	3.00 dB
Mismatch loss (VSWR $\approx$ 1.6:1)	$\approx$	0.25 dB
Actual Gain		16.55

Efficiency $\approx$ 17.84 dB - 16.55 dB $\approx$ 1.29 dB $\approx$ 74%

Again, loss resulting in the 74% efficiency can be attributed to dielectric loss and feedline radiation. The high amount of loss attributed to the waveguide/microstrip adaptor was due to the use of steel tuning screws in the waveguide. This loss was reduced to less than 1.0 dB when the steel screws were replaced with gold-plated screws.

4.3 WAVEGUIDE IRIS FED SCALED ARRAY

A third test antenna using the scaled 4x4 element array and the iris-type waveguide feed was fabricated and tested. Measured E and H plane radiation patterns of this antenna are shown in Figures 4-11 and 4-12. Results were not very encouraging. This

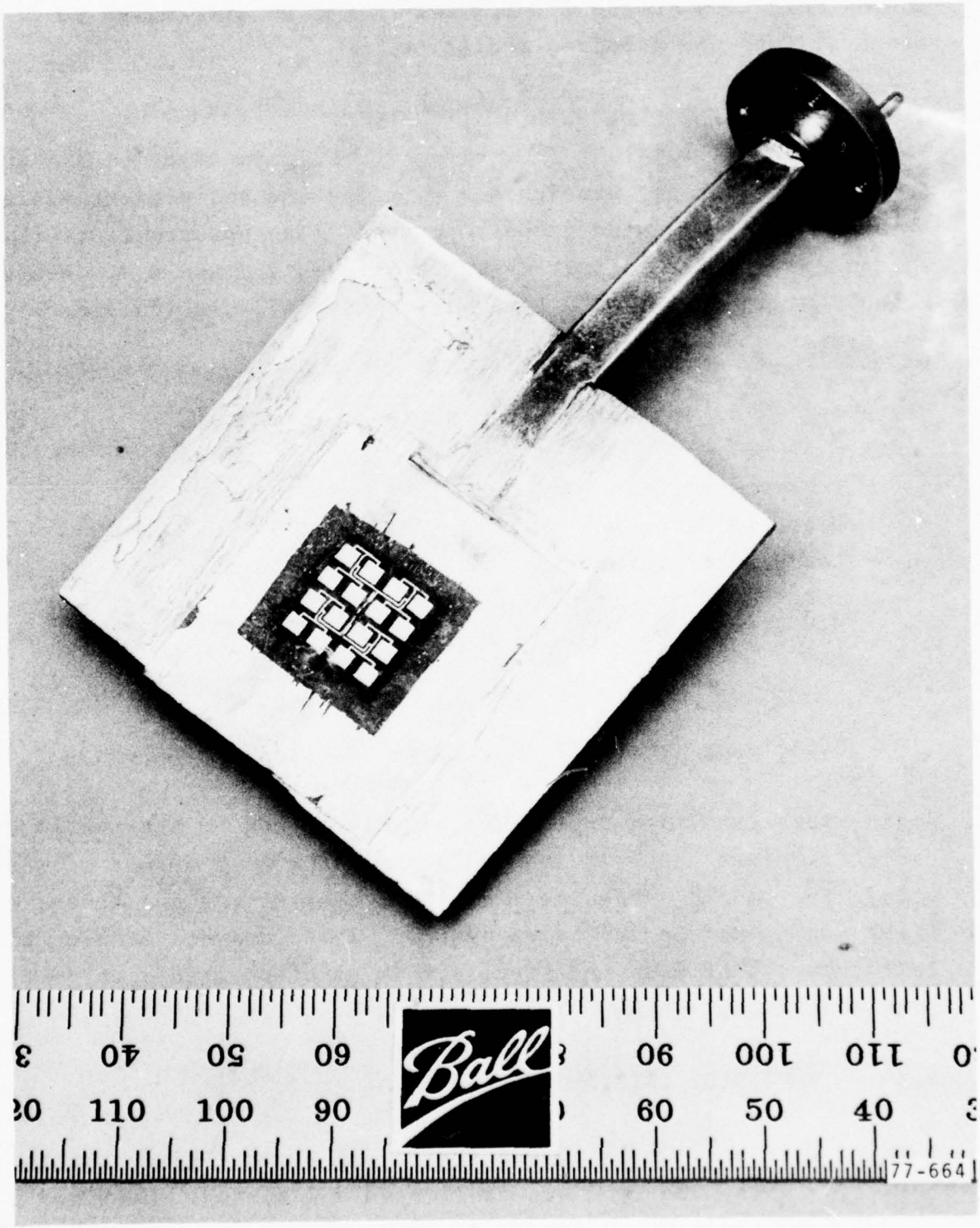

Figure 4-7 Waveguide Probe Fed Array (Front View)

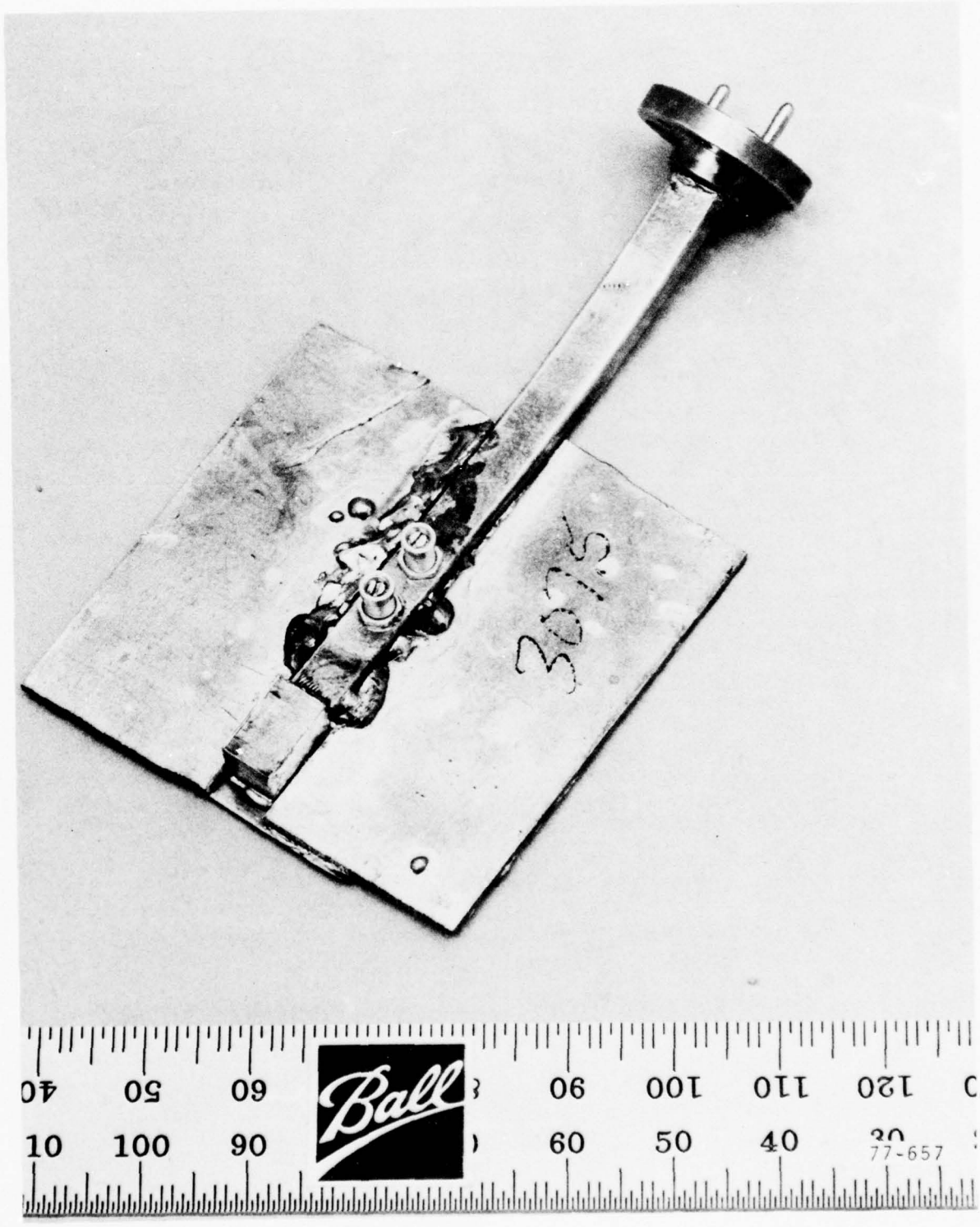

Figure 4-8 Waveguide Probe Fed Array (Back View)

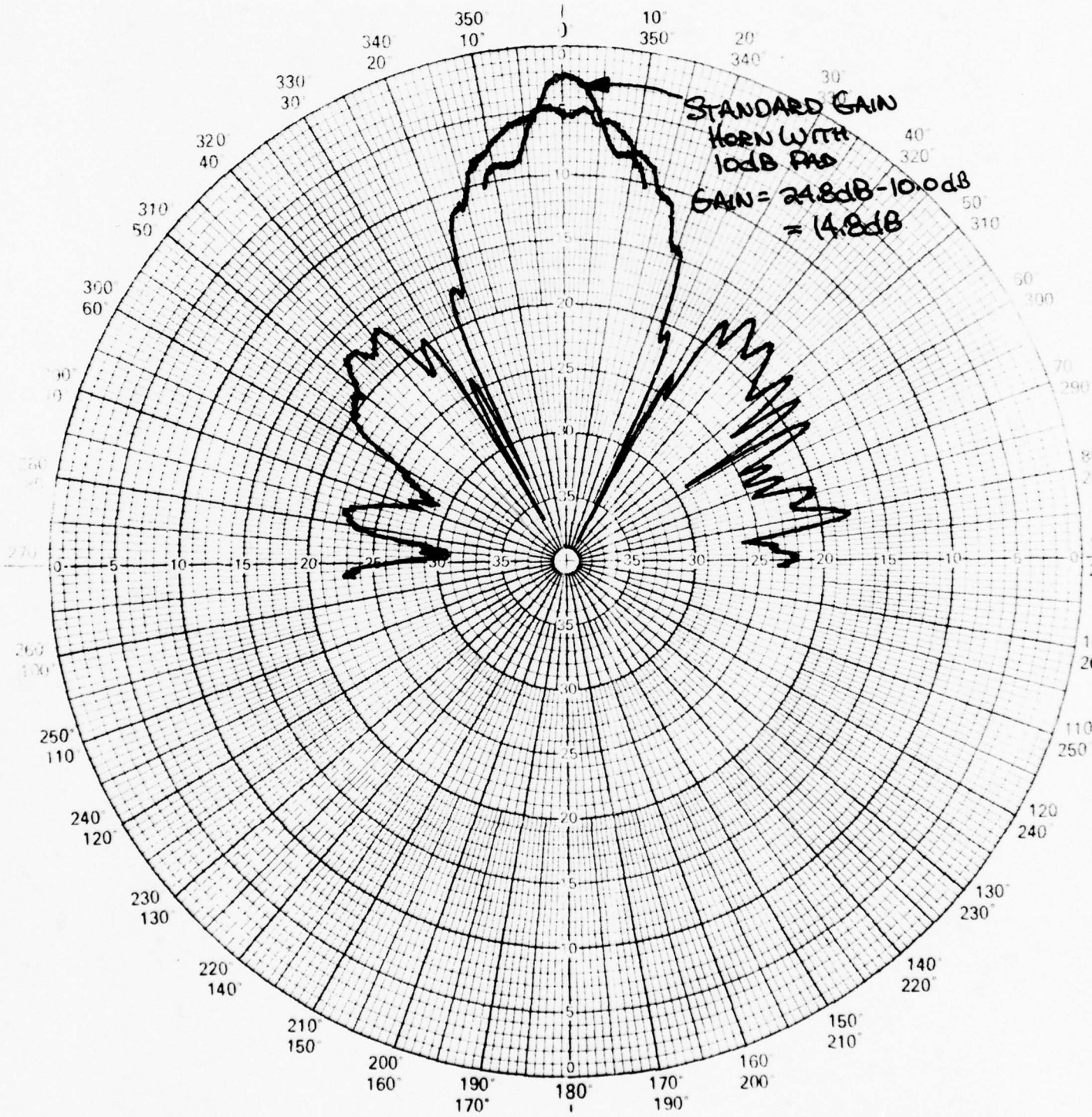

Figure 4-9 E-Plane Radiation Pattern (36.6 GHz) WG Probe Fed

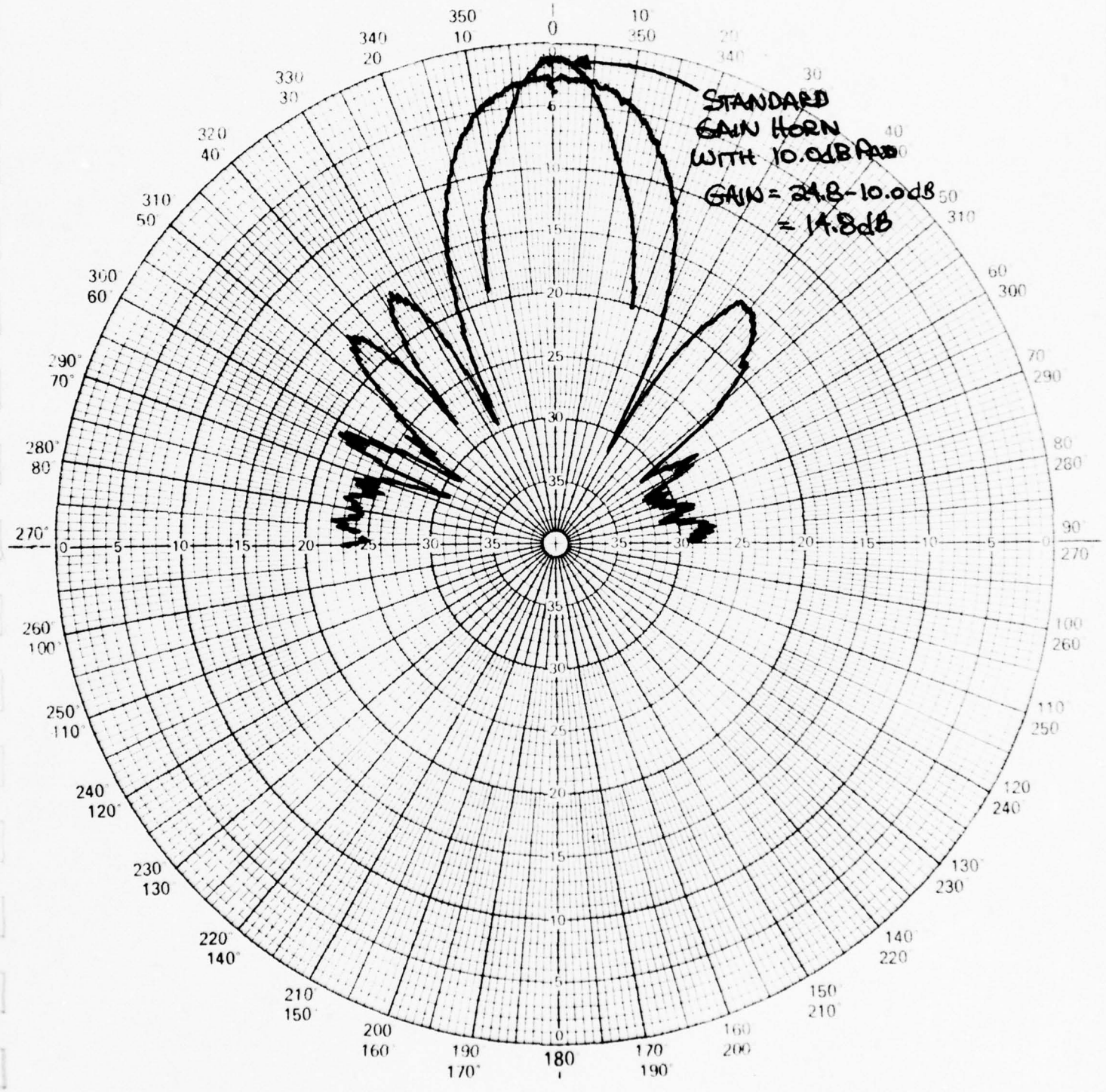

Figure 4-10 H-Plane Radiation Pattern (36.6 GHz) WG Probe Fed

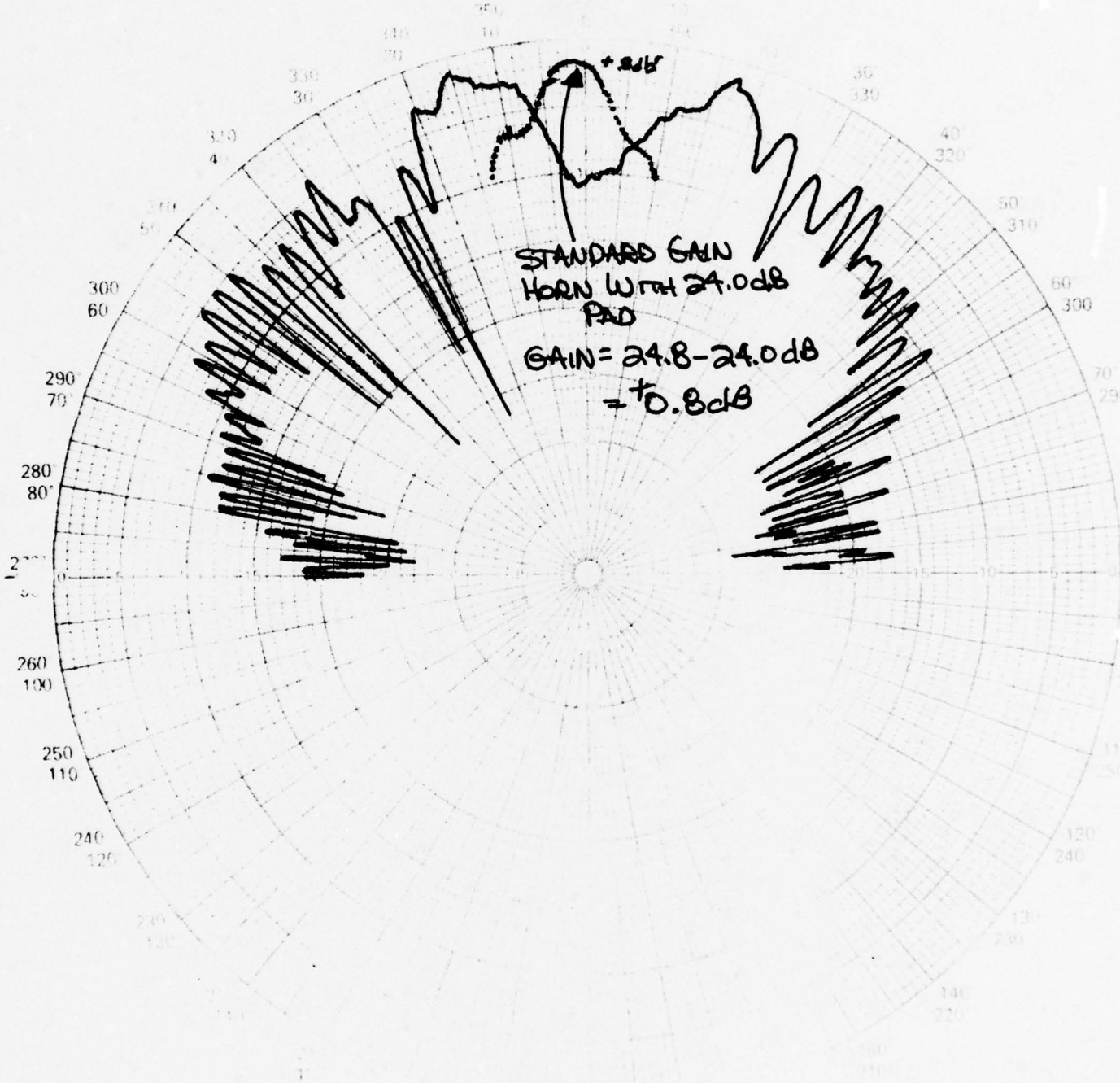

Figure 4-11 E-Plane Radiation Pattern (36.6 GHz) WG Iris Fed

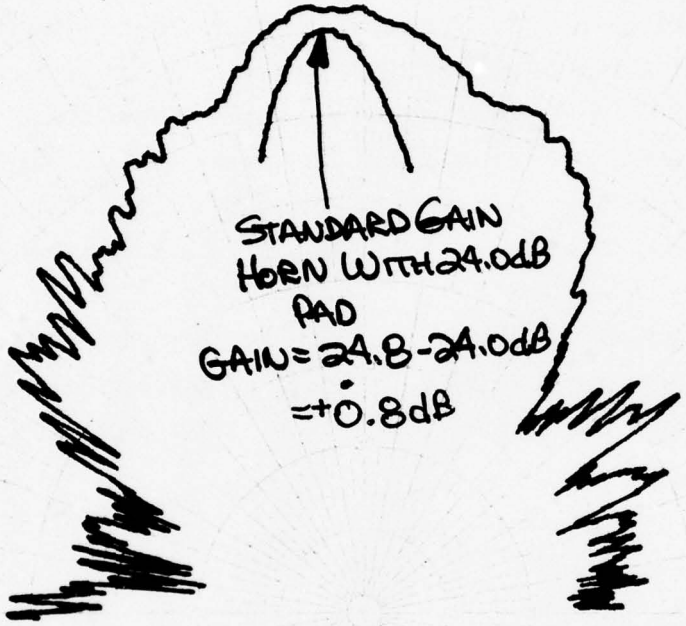

Figure 4-12 H-Plane Radiation Pattern (36.6 GHz) WG Iris Fed

can be attributed to the basic array design, through which feed-line dimensions are predetermined. This does not allow optimum sizing of the iris, thereby degrading impedance matching and transition performance. The severe pattern degradation observed in Figure 4-11 can result if the transition does not produce the theoretical 180° phase difference in the feed lines (see Section 2.2). Since the two major feed lines are phased 180° to balance the transition phase shift, an overhead null will appear in one pattern plane if the transition is not functioning properly.

Since verification of array feasibility was the basic purpose of the study, development of the iris-type waveguide transition was discontinued and the probe-type transition was used in remaining applications.

4.4 COAX FED ARRAY, NEW FEED SYSTEM

Analysis of the scaled 4x4 element array indicated that the array feed system contained the largest potential for improved performance. This conclusion was arrived at for two reasons: first, the scaled version contained impedance matching transformers only at the first power division points. The remaining two power division junctions were unmatched. Second, all feed line corners were square, possibly contributing to spurious radiation.

For these reasons, a feed system was designed having matching transformers at all power division junctions. These transformers were tapered, and all sharp corner were rounded to reduce the possibility of spurious radiation. This array was etched on 10 mil Duroid 5880 having a 1/4 oz. (0.4 mil) copper cladding.

Measured E and H plane patterns are shown in Figure 4-13 and 4-14.

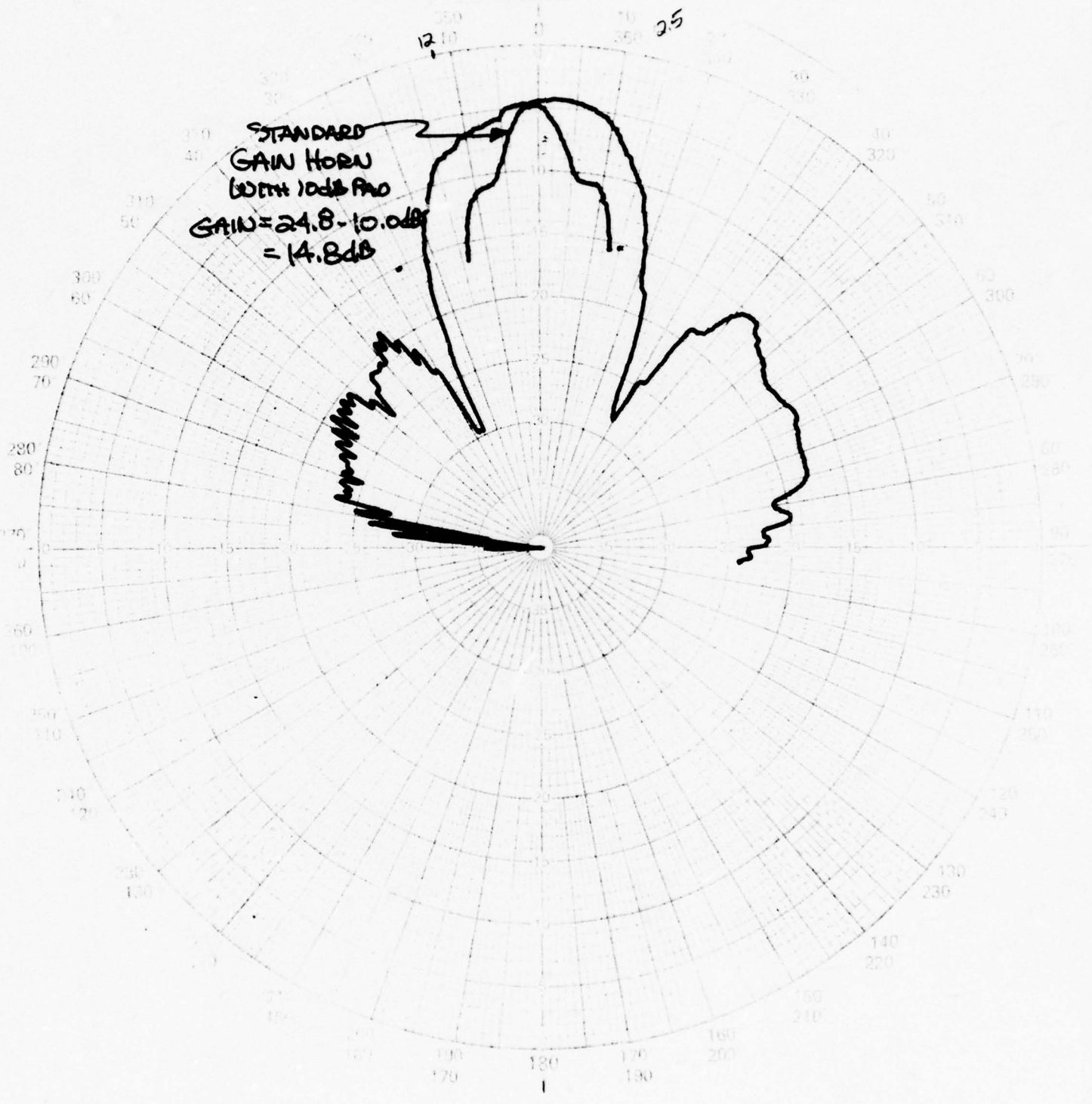

Figure 4-13 E-Plane Radiation Pattern (36.6 GHz) Coax Fed, New Feed System

11.5

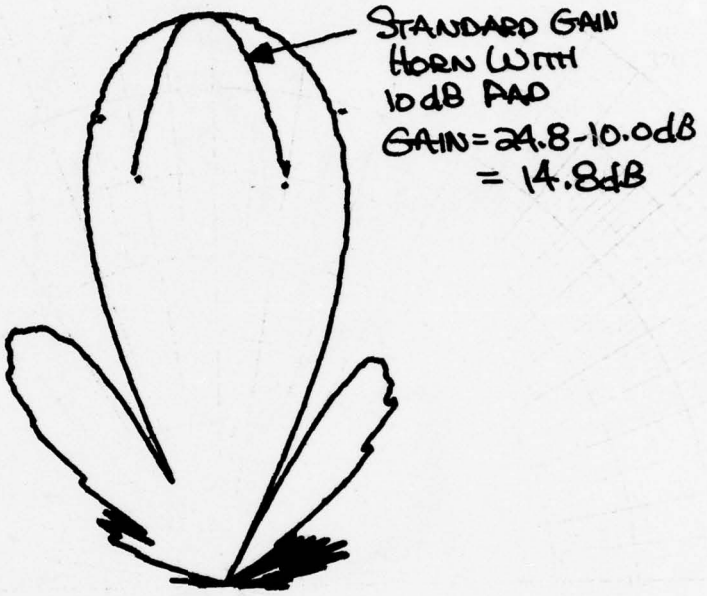

Figure 4-14 H-Plane Radiation Pattern (36.6 GHz) Coax Fed, New Feed System

An analysis of array performance follows:

Theoretical Gain		17.84 dB
Measured Gain		14.80 dB
Loss in Connector	≈	0.20 dB
Mismatch Loss (VSWR 1.9:1)	≈	0.45
Actual Gain		15.45 dB

Efficiency ≈ 17.84 dB - 15.45 dB ≈ 2.39 dB ≈ 58%

The reduced efficiency of this array indicates that tolerances of feed line parameters are too sensitive to allow design by formulas used at lower frequencies. It is expected that if taken through development at a lower frequency, this feed system design will result in an improvement in efficiency over the arrays described in Sections 4.1 and 4.2.

4.5 35 GHz ARRAY SUMMARY

Table 4-1 is a summary of investigated array performance.

Table 4-1
ARRAY PERFORMANCE SUMMARY

(36.6 GHz)

	Coax Fed/ Scaled	Waveguide Probe Fed/ Scaled	Coax Fed/ New Feed System
Efficiency	77%	74%	58%
Gain			
• Theoretical	17.84 dB	17.84 dB	17.84 dB
• Measured	16.70 dB	16.55 dB	15.45 dB
Relative Bandwidth	>400 MHz	>400 MHz	>400 MHz
Pattern Quality	Excellent	Good	Good
Sidelobe Level			
• E-Plane	≈ -15.0 dB	≈ -11.5 dB	≈ -11.0 dB
• H-Plane	≈ -12.0 dB	≈ -13.0 dB	≈ -14.5 dB
VSWR	1.7:1	1.6:1	1.9:1

Section 5
60 GHz 4x4 ELEMENT ARRAYS

5.1 WAVEGUIDE PROBE FED SCALED ARRAY

Two versions of the 60 GHz 4x4 element arrays were fabricated and tested. One was a scaled version of the array developed at 2.7 GHz. This is the antenna shown in the lower center of Figure 5-1. The other was a scaled version of the array having a modified feed network developed at 35 GHz. This array is shown in the upper center of Figure 5-1.

The scaled array was etched on 5 mil Duroid 5880 having a 1/4 oz. (0.4 mil) copper cladding and was fed using the waveguide probe technique. E and H plane radiation patterns of this antenna are shown in Figures 5-2 and 5-3. Theoretical computer generated radiation patterns of this array appear in Figures 5-4 and 5-5. The array actually operates at 57.05 GHz.

Following is an analysis of the array performance:

Theoretical Gain		17.83 dB
Measured Gain		8.00 dB
Loss in W/G microstrip transition	$\approx$	0.70 dB
Mismatch loss (VSWR 1.3:1)	$\approx$	0.10 dB
Actual Gain		9.8 dB

Efficiency $\approx$ 17.83 dB - 9.80 dB $\approx$ 8.03 dB $\approx$ 16%

Since etching tolerances and fabrication techniques become extremely critical in the 60 GHz region, it is expected that a considerable portion of the efficiency loss can be attributed to these areas. It would appear that further refinements in

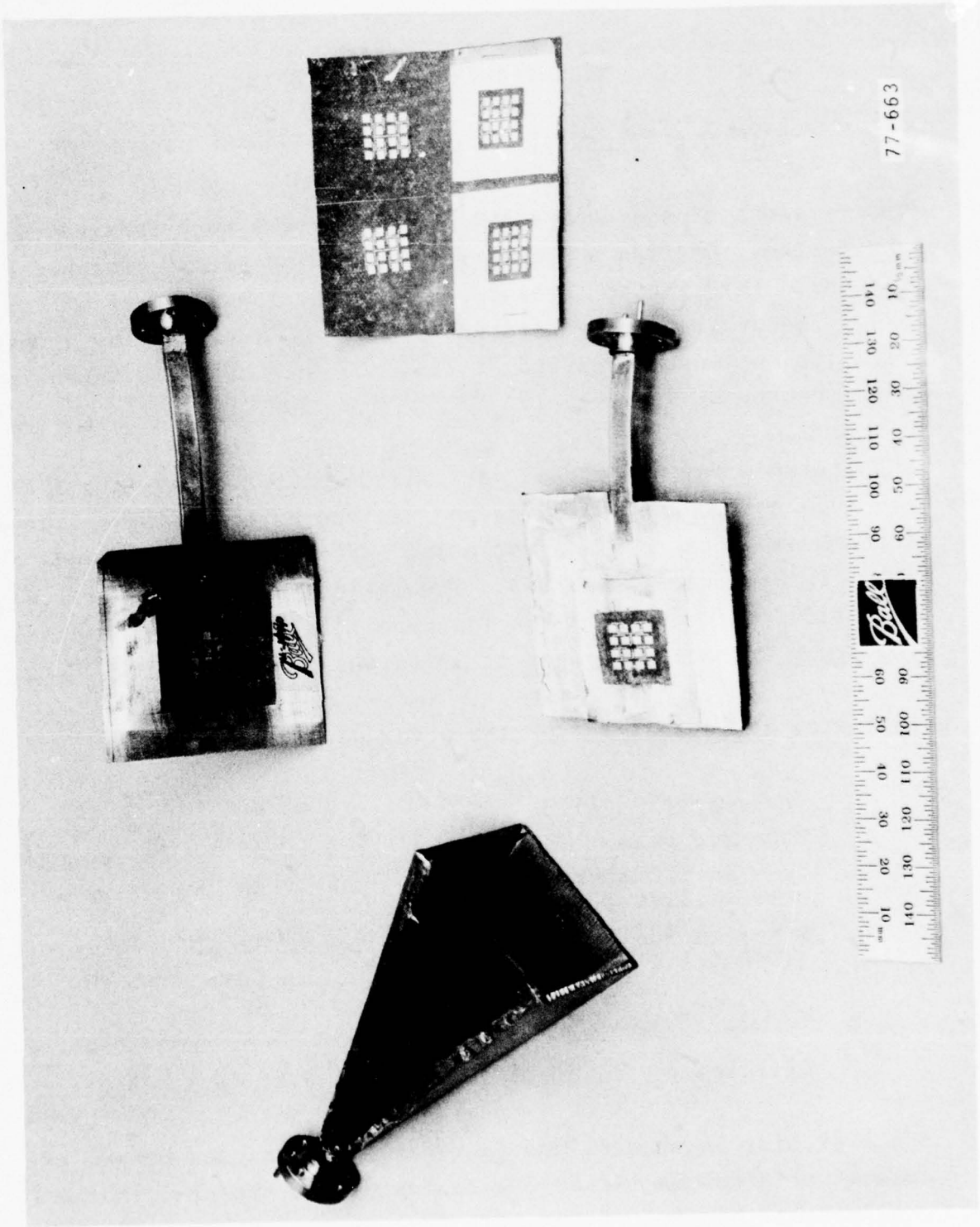

Figure 5-1 60 GHz Arrays

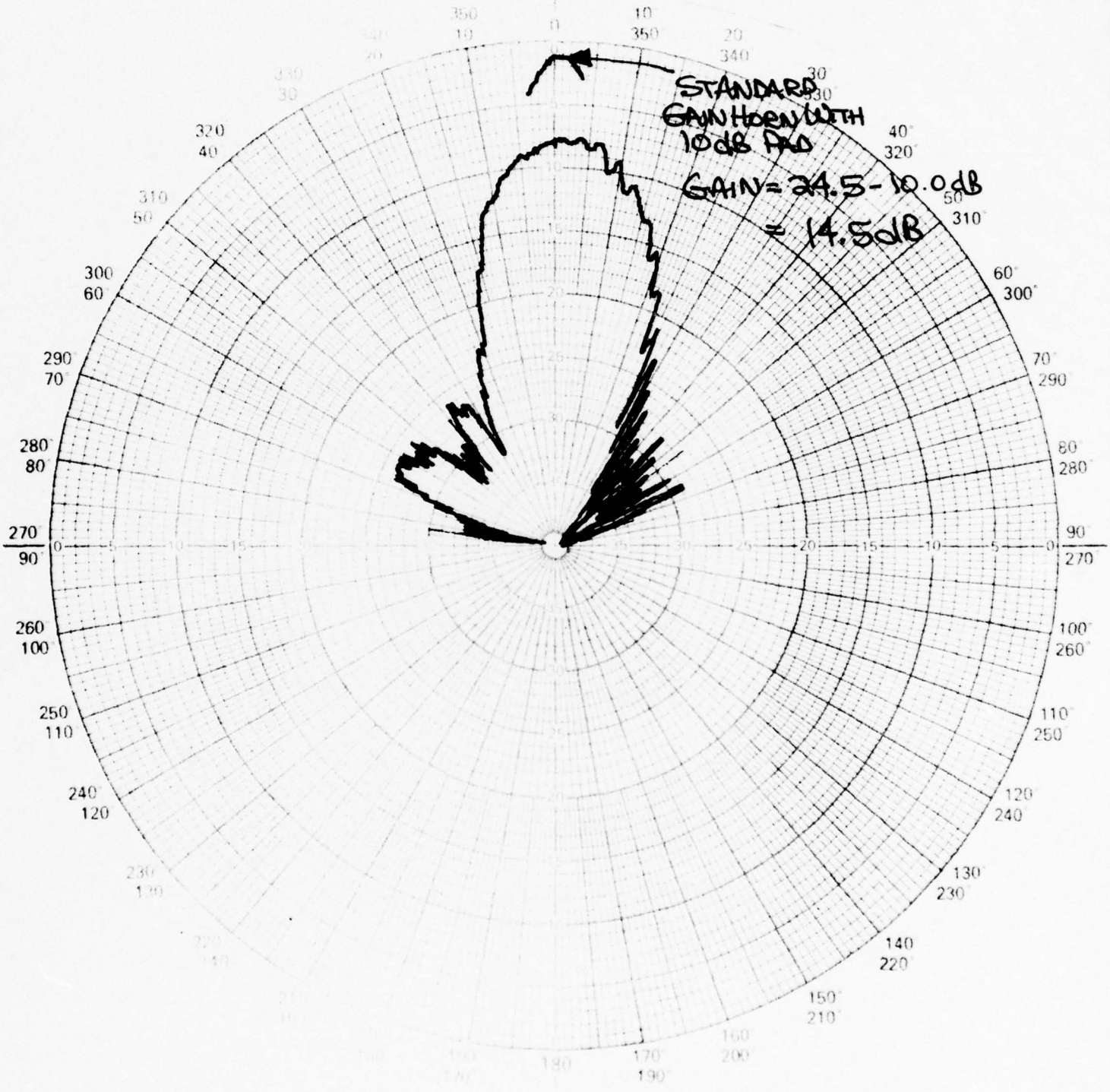

Figure 5-2 E-Plane Radiation Pattern (57.05 GHz) WG Probe Fed

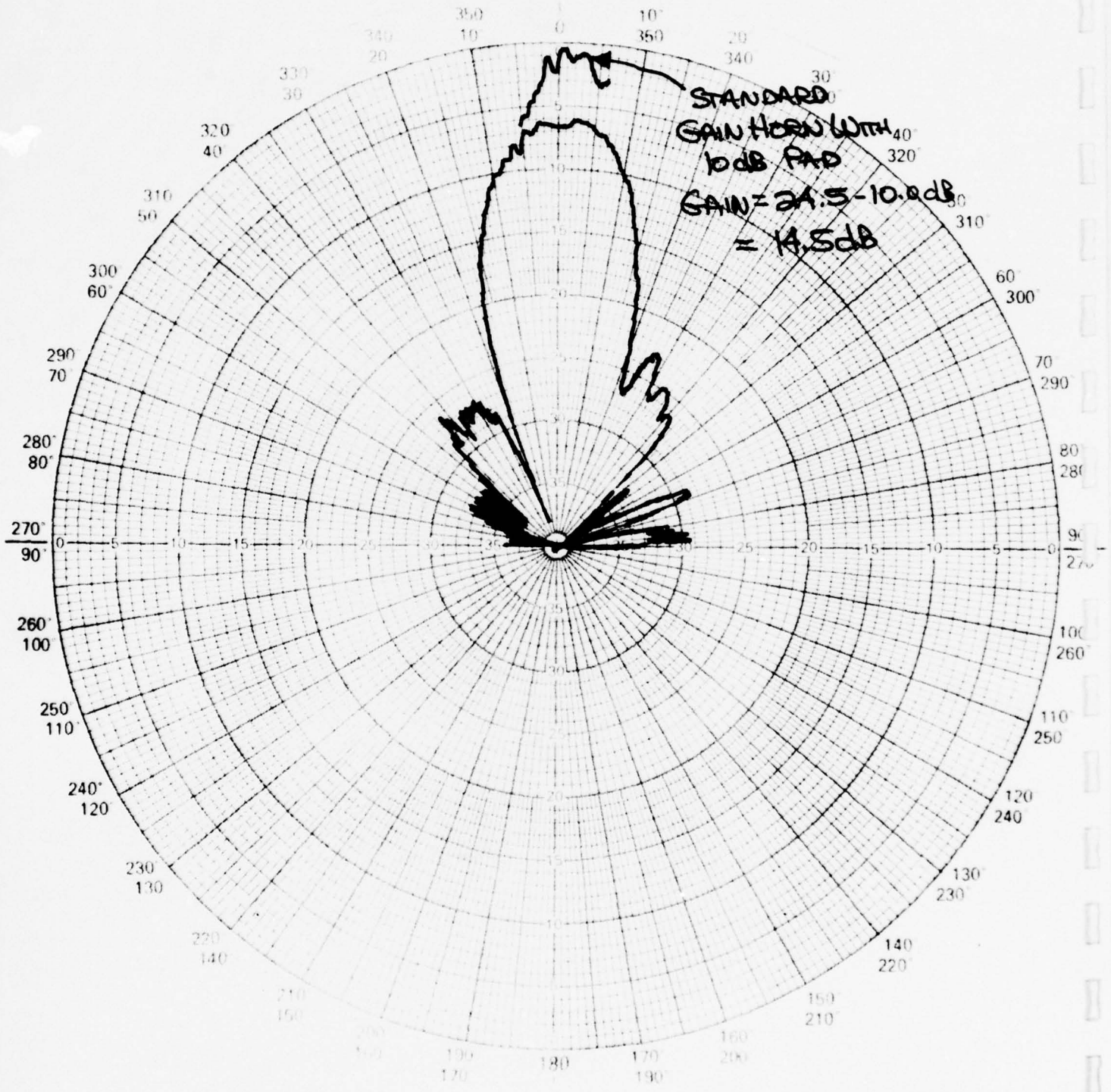

Figure 5-3 H-Plane Radiation Pattern (57.05 GHz) WG Probe Fed

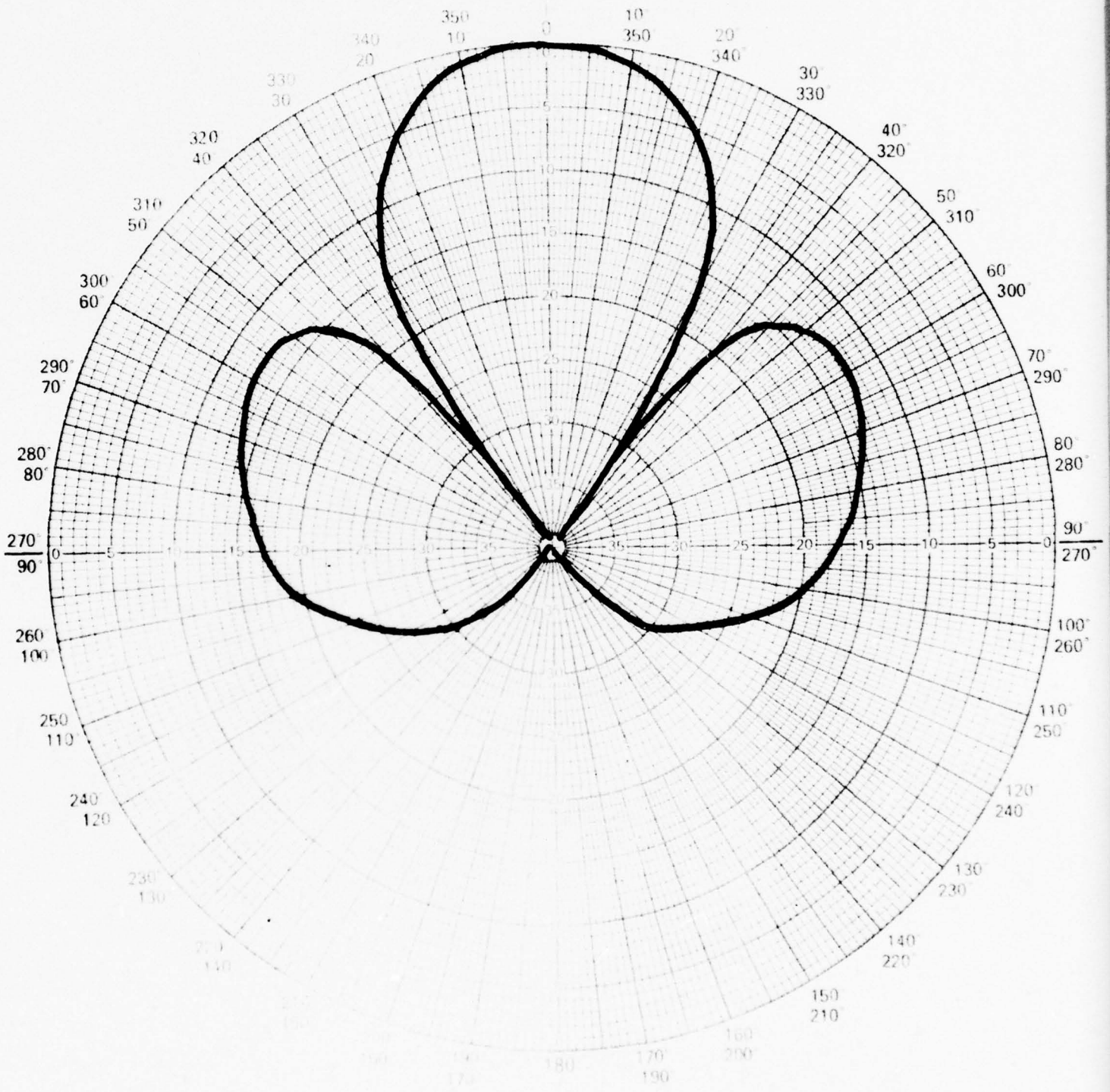

Figure 5-4 Computed E-Plane Radiation Pattern (57.05 GHz)

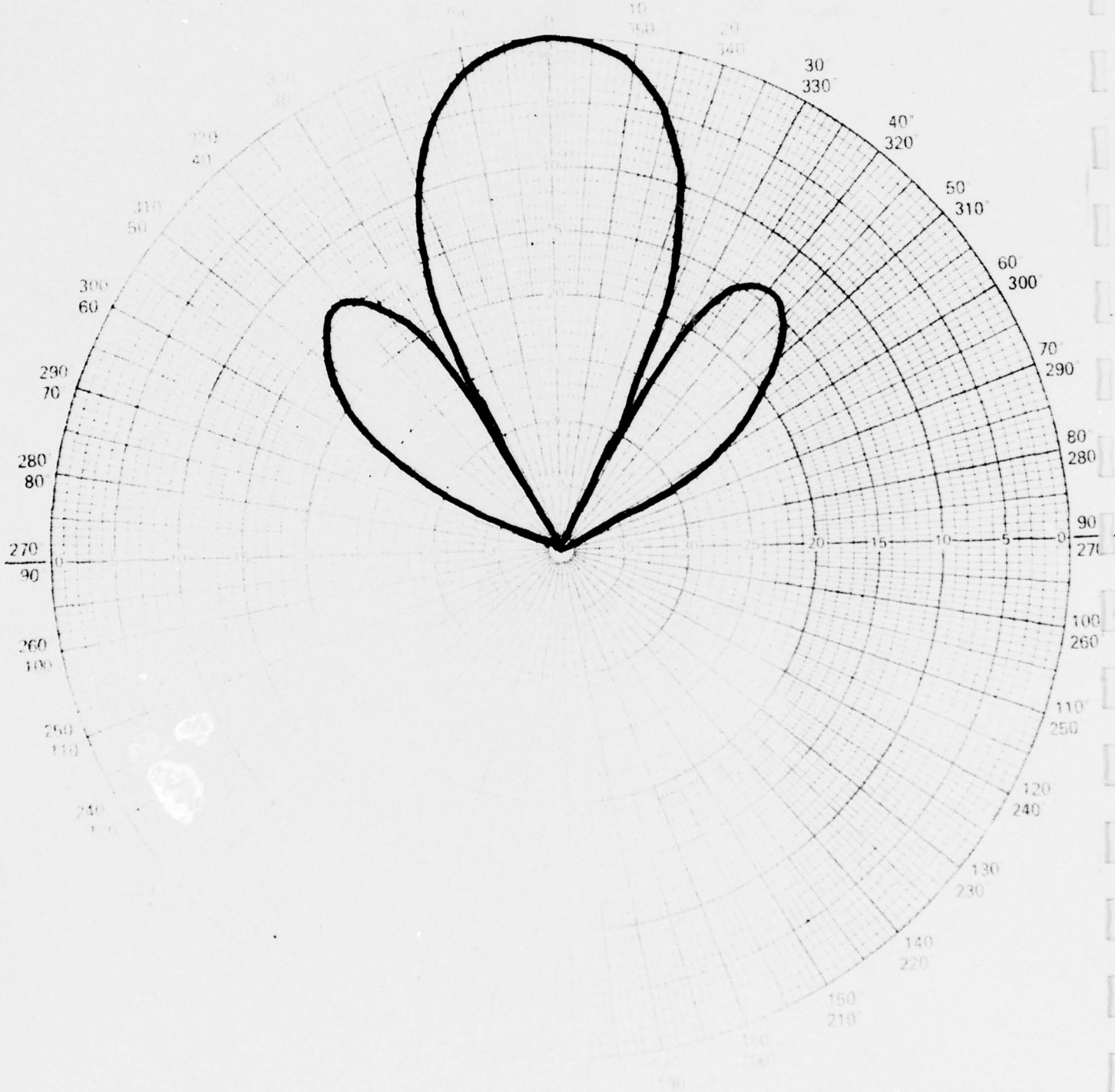

Figure 5-5 Computed H-Plane Radiation Pattern (57.05 GHz)

etching and fabrication will greatly improve antenna performance.

5.2 WAVEGUIDE PROBE FED ARRAY, NEW FEED SYSTEM

A second array was fabricated and tested using a scaled negative of the array using the revised feed system developed at 35 GHz. This array was also etched on 5 mil Duroid 5880 having a 1/4 oz. (0.4 mil) copper cladding. The array operated at approximately 57.4 GHz. Measured E and H plane radiation patterns of this array are shown in Figures 5-6 and 5-7. These patterns compare quite well with the theoretical patterns of Figures 5-4 and 5-5.

To facilitate fabrication of this antenna, a short piece of 0.085" semirigid coaxial cable was used between the waveguide/coax transition and the actual array. Since the array functioned relatively well, it was assumed there were no moding problems in the coaxial cable.

Following is an analysis of the array performance:

Theoretical Gain		17.83 dB
Measured Gain		15.76 dB
Loss in waveguide/coax transition	$\approx$	0.50 dB
Loss in 0.6" of coax cable	$\approx$	0.11 dB
Mismatch loss (VSWR 1.8:1)	$\approx$	0.37 dB
Actual Gain		16.74 dB

Efficiency $\approx$ 17.83 dB - 16.74 dB $\approx$ 1.09 dB $\approx$ 78%

The efficiency of this array is directly comparable with experimental results obtained at 35 GHz. This efficiency value suggests an undetected problem with the scaled array or a malfunctioning of equipment during pattern measurements.

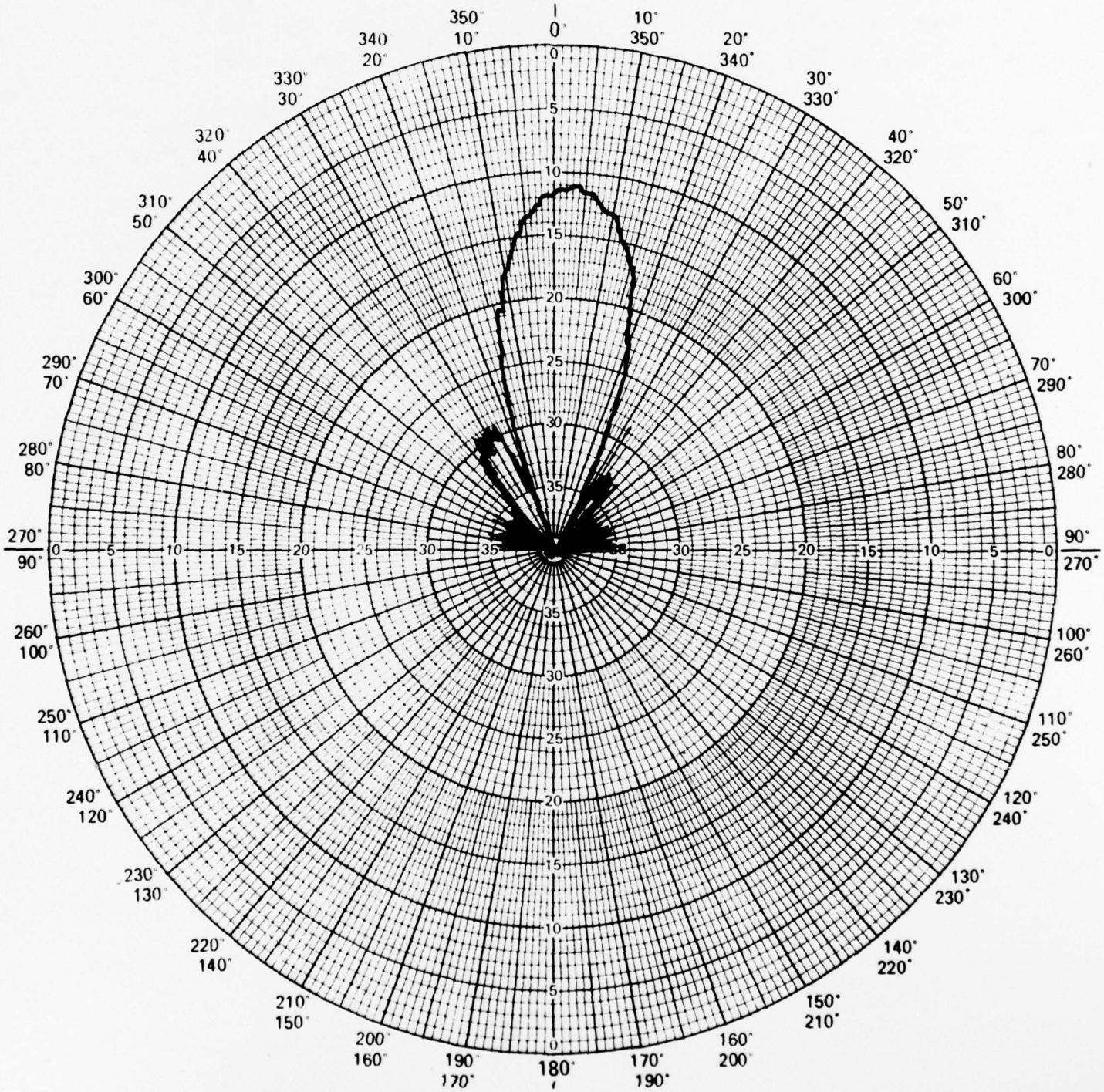

Figure 5-7 H-Plane Radiation Pattern (57.4 GHz) WG Probe Fed, New Feed System

The similar efficiency values at both 35 and 60 GHz indicate that the advantages of the microstrip approach to antenna systems do not deteriorate in the millimeter wave range.

5.3 60 GHz ARRAY SUMMARY

Table 5-1 is a summary of investigated array performance.

Table 5-1
ARRAY PERFORMANCE SUMMARY

(57.05 & 57.4 GHz)

	Waveguide Probe Fed/Scaled	Waveguide Probe Fed/New Feed System
Efficiency	16%	78%
Gain		
• Theoretical	17.83 dB	17.83 dB
• Measured	9.80 dB	16.74 dB
Relative Bandwidth	>800 MHz	>800 MHz
Pattern Quality	Good	Excellent
Sidelobe Level		
• E-Plane	≈ -18.0 dB	≈ -12.2 dB
• H-Plane	≈ -17.0 dB	≈ -18.0 dB
VSWR	1.3:1	1.8:1

Section 6
EQUIPMENT

6.1 TEST SETUP

To facilitate impedance and radiation pattern measurements, a test fixture was fabricated to accommodate the Impatt source, attenuator, and frequency meter for both the 35 and 60 GHz applications. A photograph of this fixture is shown in Figure 6-1.

In addition, a second horn antenna was fabricated for each frequency for use as the R.F. source antenna. This made available the purchased standard gain horns for use as references in making comparative gain measurements.

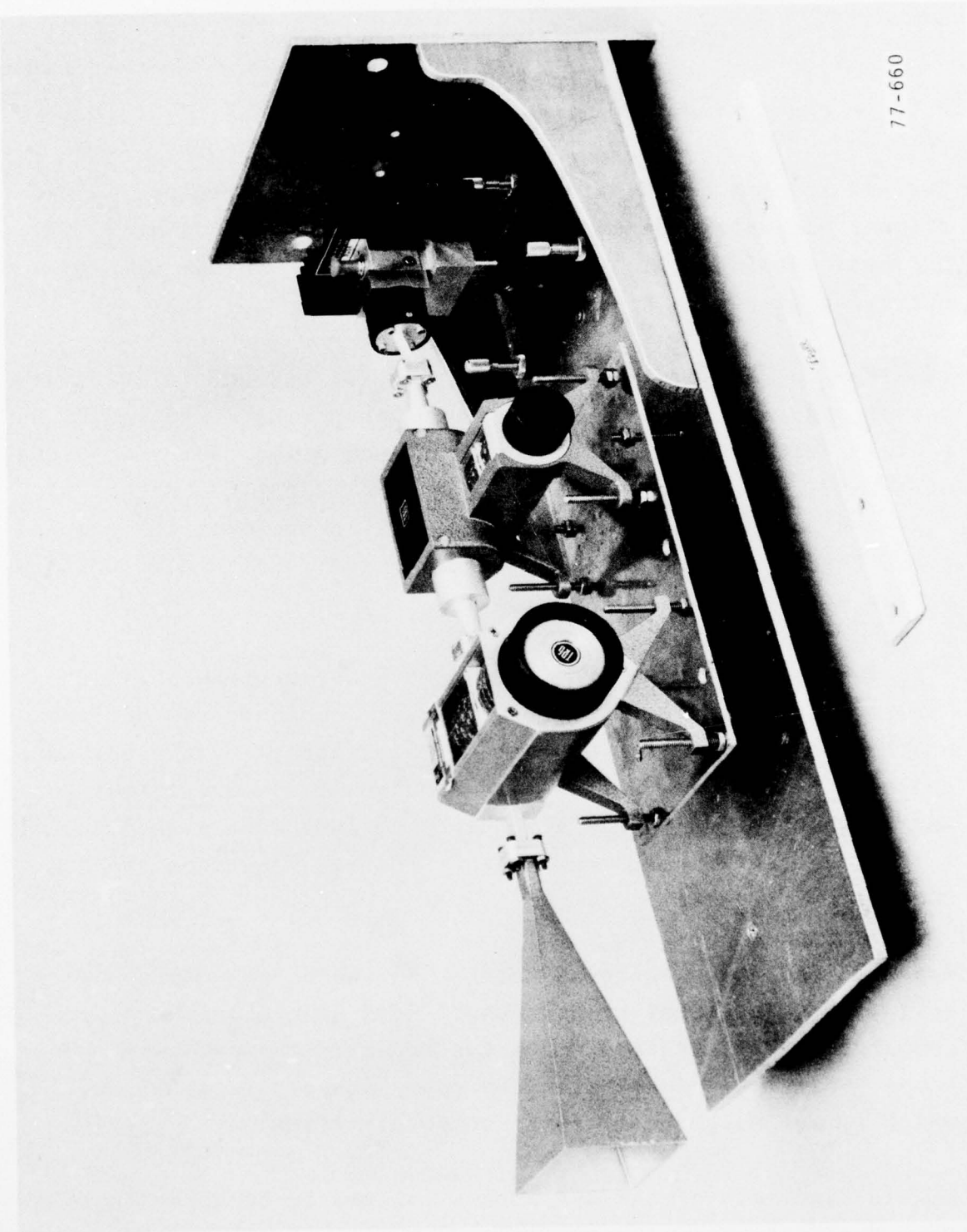

Figure 6-1 R.F. Test Fixture

Section 7
CONCLUSIONS AND RECOMMENDATIONS

7.1 CONCLUSIONS

Overall results of the study are extremely encouraging. A 4x4 element microstrip array having an efficiency of 77% at 35 GHz has been developed, fabricated, and tested. Similar arrays operating at 60 GHz have achieved efficiencies of 78%.

Two types of substrate material, Polyguide and Duroid 5880, were analyzed during the 35 GHz portion of this study. Polyguide has a dielectric constant of 2.26 and a dissipation factor of 0.00027 at X-band, while the Duroid 5880 has a dielectric constant of 2.20 and a dissipation factor of 0.0009. Because of its composition, the dielectric constant of Polyguide is also more uniform within a given area of material.

This data suggests that Polyguide should be a preferable substrate material. Test results, however, indicate the performance of the two materials is essentially identical. Duroid 5880 was chosen for the remaining testing because it is much easier to work with. Polyguide has a tendency to curl when etched and also melts when heated, as occurs when soldering feedlines and connectors to the array.

Measured radiation patterns both at 35 and 60 GHz compare very well with theoretical predictions. Main beam beamwidths are comparable and sidelobes and nulls occur in the predicted positions. First sidelobes are down approximately 12 to 13 dB, which agrees with theory for a uniformly illuminated array.

Usable bandwidth of the 4x4 arrays appears to be approximately one percent, which is comparable with typical microstrip antennas at lower frequencies.

7.2 RECOMMENDATIONS

Two recommendations should be stressed in further development of microstrip millimeter wave antennas. First, as mentioned in Section 3, it is essential to use substrate materials whose copper cladding is as thin as possible (i.e., 1/4 oz. or 0.4 mil). This thin cladding greatly enhances the ability to maintain close tolerances while reducing the effects of undercutting during etching.

Secondly, to obtain maximum performance, millimeter antennas should first be fabricated and optimized at a lower scale frequency. This allows a much greater ability to refine antenna performance than is available at the millimeter frequencies, where measurement limitations inhibit accurate determination of individual component performance.

DISTRIBUTION LIST

101 DEFENSE DOCUMENTATION CENTER
ATTN: DDC-TCA
CAMERON STATION (BLDG5)
*012 ALEXANDRIA, VA 22314

102 DIRECTOR
NATIONAL SECURITY AGENCY
ATTN: TDL
001 FORT GEORGE G. MEADE, MD 20755

103 CODE R123, TECH LIBRARY
DCA DEFENSE COMM ENGRG CTR
1860 WIEHLE AVE
001 RESTON, VA 22090

104 DEFENSE COMMUNICATIONS AGENCY
TECHNICAL LIBRARY CENTER
CODE 205 (P. A. TOLOVI)
001 WASHINGTON, DC 20305

200 OFFICE OF NAVAL RESEARCH
CODE 427
001 ARLINGTON, VA 22217

203 GIDEP ENGINEERING & SUPPORT DEPT
TE SECTION
PO BOX 398
001 NORCO, CA 91760

205 DIRECTOR
NAVAL RESEARCH LABORATORY
ATTN: CODE 2627
001 WASHINGTON, DC 20375

206 COMMANDER
NAVAL ELECTRONICS LABORATORY CENTER
ATTN: LIBRARY
001 SAN DIEGO, CA 92152

207 CDR, NAVAL SURFACE WEAPONS CENTER
WHITE OAK LABORATORY
ATTN: LIBRARY, CODE WX-21
001 SILVER SPRING, MD 20910

210 COMMANDANT, MARINE CORPS
HQ, US MARINE CORPS
ATTN: CODE LMC
002 WASHINGTON, DC 20380

211 HQ, US MARINE CORPS
ATTN: CODE INTS
001 WASHINGTON, DC 20380

212 COMMAND, CONTROL & COMMUNICATIONS DIV
DEVELOPMENT CENTER
MARINE CORPS DEVELOPMENT & EDUC COMD
001 QUANTICO, VA 22134

* Decrease to 2 copies if report is not releasable to public. See DODMR 70-31 for types of reports not to be sent to DDC

215 NAVAL TELECOMMUNICATIONS COMMAND
TECHNICAL LIBRARY, CODE 91L
4401 MASSACHUSETTS AVENUE, NW
001 WASHINGTON, DC 20390

217 NAVAL AIR SYSTEMS COMMAND
CODE: AIR-5332
004 WASHINGTON, DC 20360

300 AUL/LSE 64-285
001 MAXWELL AFB, AL 36112

301 ROME AIR DEVELOPMENT CENTER
ATTN: DOCUMENTS LIBRARY (TILD)
001 GRIFFISS AFB, NY 13441

304 AIR FORCE GEOPHYSICS LAB
L. G. HANSCOM AFB
ATTN: LIR
001 BEDFORD, MA 01730

307 HQ ESD (DRI)
L. G. HANSCOM AFB
001 BEDFORD, MA 01731

310 HQ, AFCS
ATTN: EPECRW MAIL STOP 105B
001 RICHARDS-GEBAUR AFB, MO 64030

312 HQ, AIR FORCE ELECTRONIC WARFARE CENTER
ATTN: SURP
002 SAN ANTONIO, TX 78243

314 HQ, AIR FORCE SYSTEMS COMMAND
ATTN: DLCA
ANDREWS AFB
001 WASHINGTON, DC 20331

403 CDR, US ARMY MISSILE COMMAND
REDSTONE SCIENTIFIC INFO CENTER
ATTN: CHIEF, DOCUMENT SECTION
002 REDSTONE ARSENAL, AL 35809

406 COMMANDANT
US ARMY AVIATION CENTER
ATTN: ATZQ-D-MA
003 FORT RUCKER, AL 36362

408 COMMANDANT
US ARMY MILITARY POLICE SCHOOL
ATTN: ATSJ-CD-M-C
003 FORT MCCLELLAN, AL 36201

417 COMMANDER
US ARMY INTELLIGENCE CENTER & SCHOOL
ATTN: ATSI-CD-MD
002 FORT HUACHUCA, AZ 85613

418 COMMANDER
HQ FORT HUACHUCA
ATTN: TECHNICAL REFERENCE DIV
001 FORT HUACHUCA, AZ 85613

419 COMMANDER
US ARMY ELECTRONIC PROVING GROUND
ATTN: STEEP-MT
002 FORT HUACHUCA, AZ 85613

420 COMMANDER
USASA TEST & EVALUATION CENTER
ATTN: IAO-CDR-T
001 FORT HUACHUCA, AZ 85613

421 COMMANDER
HQ US ARMY COMMUNICATIONS COMMAND
ATTN: CC-OPS-SM
001 FORT HUACHUCA, AZ 85613

3

432 DIR, US ARMY AIR MOBILITY R&D LAB
ATTN: T. GOSSETT, BLDG 207-5
NASA AMES RESEARCH CENTER
001 MOFFETT FIELD, CA 94035

436 HQDA(DAMO-TCE)
002 WASHINGTON, DC 20310

437 DEPUTY FOR SCIENCE & TECHNOLOGY
OFFICE, ASSIST SEC ARMY (R&D)
001 WASHINGTON, DC 20310

438 HQDA(DAMA-ARP/DR. F. D. VERDERAME)
001 WASHINGTON, DC 20310

470 DIRECTOR OF COMBAT DEVELOPMENTS
US ARMY ARMOR CENTER
ATTN: ATZK-CD-MS
002 FORT KNOX, KY 40121

473 COMMANDANT
US ARMY ORDNANCE SCHOOL
ATTN: ATSL-CD-OR
002 ABERDEEN PROVING GROUND, MD 21005

475 CDR, HARRY DIAMOND LABORATORIES
ATTN: LIBRARY
2800 POWDER MILL ROAD
001 ADELPHI, MD 20783

477 DIRECTOR
US ARMY BALLISTIC RESEARCH LABS
ATTN: DRXBR-LB
001 ABERDEEN PROVING GROUND, MD 21005

478 DIRECTOR
US ARMY BALLISTIC RESEARCH LABS
ATTN: DRXBR-CA (DR. L. VANDEKIEFT)
001 ABERDEEN PROVING GROUND, MD 21005

479 DIRECTOR
US ARMY HUMAN ENGINEERING LABS
001 ABERDEEN PROVING GROUND, MD 21005

482 DIRECTOR
US ARMY MATERIEL SYSTEMS ANALYSIS ACTY
ATTN: DRXSY-T
001 ABERDEEN PROVING GROUND, MD 21005

507 CDR, US ARMY AVIATION SYSTEMS COMMAND
ATTN: DRSAV-E
PO BOX 209
001 ST. LOUIS, MO 63166

512 COMMANDER
PICATINNY ARSENAL
ATTN: SARPA-ND-A-4 (BLDG 95)
001 DOVER, NJ 07801

514 DIRECTOR
JOINT COMM OFFICE (TRI-TAC)
ATTN: TT-AD(TECH DOCU CEN)
001 FORT MONMOUTH, NJ 07703

515 PROJECT MANAGER, REMBASS
ATTN: DRCPM-RBS
002 FORT MONMOUTH, NJ 07703

516 PROJECT MANAGER, NAVCON
ATTN: DRCPM-NC-TM
BLDG 2539
001 FORT MONMOUTH, NJ 07703

517 COMMANDER
US ARMY SATELLITE COMMUNICATIONS AGCY
ATTN: DRCPM-SC-3
002 FORT MONMOUTH, NJ 07703

518 TRI-TAC OFFICE
ATTN: CSS (DR. PRITCHARD)
001 FORT MONMOUTH, NJ 07703

531 CDR, US ARMY RESEARCH OFFICE
ATTN: DRXRO-IP
PO BOX 12211
001 RESEARCH TRIANGLE PARK, NC 27709

533 COMMANDANT
US ARMY INST FOR MILITARY ASSISTANCE
ATTN: ATSU-CTD-MO
001 FORT BRAGG, NC 28307

536 COMMANDER
US ARMY ARCTIC TEST CENTER
ATTN: STEAC-TD-MI
002 APO SEATTLE 98733

537 CDR, US ARMY TROPIC TEST CENTER
ATTN: STETC-MO-A (TECH LIBRARY)
DRAWER 942
001 FORT CLAYTON, CANAL ZONE 09827

542 COMMANDANT
US ARMY FIELD ARTILLERY SCHOOL
ATTN: ATSFA-CTD
002 FORT SILL, OK 73503

548 COMMANDER
FRANKFORD ARSENAL
ATTN: PDS 64-4 (J. L. HELFRICH)
001 PHILADELPHIA, PA 19137

554 COMMANDANT
US ARMY AIR DEFENSE SCHOOL
ATTN: ATSA-CD-MC
001 FORT BLISS, TX 79916

555 COMMANDER
US ARMY NUCLEAR AGENCY
001 FORT BLISS, TX 79916

563 COMMANDER, DARCOM
ATTN: DRCDE
5001 EISENHOWER AVE
001 ALEXANDRIA, VA 22333

564 CDR, US ARMY SECURITY AGENCY
ATTN: IARDA-IT
ARLINGTON HALL STATION
001 ARLINGTON, VA 22212

566 CDR, US ARMY SECURITY AGENCY
ATTN: IARDA-AQ
ARLINGTON HALL STATION
001 ARLINGTON, VA 22212

572 COMMANDER
US ARMY LOGISTICS CENTER
ATTN: ATCL-MC
002 FORT LEE, VA 22801

575 COMMANDER
US ARMY TRAINING & DOCTRINE COMMAND
ATTN: ATCD-TEC
001 FORT MONROE, VA 23651

577 COMMANDER
US ARMY TRAINING & DOCTRINE COMMAND
ATTN: ATCD-TM
001 FORT MONROE, VA 23651

578 CDR, US ARMY GARRISON
VINT HILL FARMS STATION
ATTN: IAVAAF
001 WARRENTON, VA 22186

602 DIRECTOR, NIGHT VISION LABORATORY
US ARMY ELECTRONICS COMMAND
ATTN: DRSEL-NV-D
001 FORT BELVOIR, VA 22060

603 CDR/DIR, ATMOSPHERIC SCIENCES LABORATORY
US ARMY ELECTRONICS COMMAND
ATTN: DRSEL-BL-SY-S
001 WHITE SANDS MISSILE RANGE, NM 88002

605 CHIEF, AVIATION ELECTRONICS DIV (SIMO)
US ARMY ELECTRONICS COMMAND
ATTN: DRSEL-SI-AE, PO BOX 209
001 ST. LOUIS, MO 63166

606 CHIEF
INTEL MATERIEL DEV & SUPPORT OFC
ELECTRONIC WARFARE LAB, ECOM
001 FORT MEADE, MD 20755

680 COMMANDER
US ARMY ELECTRONICS COMMAND
000 FORT MONMOUTH, NJ 07703

1	DRSEL-PL-ST
1	DRSEL-VL-D
1	DRSEL-PP-I-PI
1	DRSEL-WL-D
1	DRSEL-TL-D
3	DRSEL-CT-D
1	DRSEL-BL-D
*3	DRSEL-NL-
1	DRSEL-NL- (Ofc of Record)
1	DRSEL-SI-CM
1	DRSEL-MA-MP
**2	DRSEL-MS-TI
1	DRSEL-GG-TD
2	DRSEL-PA
1	DRCPM-AA
1	DRCPM-TDS-SE
1	USMC-LNO
1	DRSEL-GS-H
1	DRSEL-RD
1	TRADOC-LNO
25	Originating Office

701 MIT - LINCOLN LABORATORY
ATTN: LIBRARY (RM A-082)
PO BOX 73
002 LEXINGTON, MA 02173

703 NASA SCIENTIFIC & TECH INFO FACILITY
BALTIMORE/WASHINGTON INTL AIRPORT
001 PO BOX 8757, MD 21240

705 ADVISORY GROUP ON ELECTRON DEVICES
201 VARICK STREET, 9TH FLOOR
002 NEW YORK, NY 10014

706 ADVISORY GROUP ON ELECTRON DEVICES
ATTN: SECY, WORKING GROUP D (LASERS)
201 VARICK STREET
002 NEW YORK, NY 10014

707 TACTEC
BATTELLE MEMORIAL INSTITUTE
505 KING AVENUE
001 COLUMBUS, OH 43201

710 KETRON, INC.
ATTN: MR. FREDERICK LEUPPERT
1400 WILSON BLVD, ARCHITECT BLDG
002 ARLINGTON, VA 22209

712 R. C. HANSEN, INC.
PO BOX 215
001 TARZANA, CA 91356

* Or number specified in contract. Add COTR's mail symbol.

** Unclassified reports only.

ADDRESSES FOR ANTENNA TEAM, 12 AUG 76

Mr. Gordon Weatherup
Rome Air Development Center
Griffiss Air Force Base
RADC/DCCN
Rome, New York 13440

Mr. James R. Scalo
NATC WST-345
Patuxent River, MD 20670

Mr. M.L. Musselman
Naval Research Laboratory
Code 5405
Washington, DC 20375

Mr. Peter Trask
NUSC
New London Laboratory
New London, CO 06320

Mr. C. Fessenden
NUSC
New London Laboratory (SA422)
New London, CO 06320

Dr. E. Miller
Lawrence Radiation Laboratory
Livermore, CA 94550

Dr. John Rockway
Naval Electronics Laboratory Center
Code 2110
San Diego, CA 92152

Mr. Richard W. Bigelow
Richards-Gebuar Air Force Base
AFCS/EPELS
Grandview, MI 64030

HQ AFCS/FFOX
Richards-Gebuar Air Force Base
ATTN: LTC Gubler
Grandview, MI 64030

Commanding Officer
US Army Mobility Equipment R&D Center
ATTN: Mr. Dallas Barr
Fort Belvoir, VA 22060

R.C. Hansen, Inc.
Box 215
Tarzana, CA 91356
(Included in Exploratory Research Distribution List)

Air Force Cambridge Rsch Lab
LG Hanscom Field
ATTN: LIR
Bedford, MA 01730